BSGF - Earth Sciences Bulletin 2021, 192, 19

https://doi.org/10.1051/bsgf/2021011

BSGF Earth Sciences Bulletin

Available online at:
www.bsgf.fr

Special Issue Orogen lifecycle: learnings and perspectives from Pyrenees, Western Mediterranean and analogues, ed. O. Lacombe, S. Tavani, A. Teixell, D. Pedreira et S. Calassou

OPEN ACCESS

Large-scale vertical movements in Cenomanian to Santonian carbonate platform in Iberia: indicators of a Coniacian pre-orogenic compressive stress

Simon Andrieu[1], Nicolas Saspiturry[2], Marine Lartigau[2], Benoit Issautier[1], Paul Angrand[3,*] and Eric Lasseur[1]

[1] BRGM-French Geological Survey, 3, avenue Claude Guillemin, BP 36009, 45060 Orléans, France
[2] Université Bordeaux Montaigne/EA 4592 Géoressources & Environnement, 1, allée Fernand Daguin, 33607 Pessac cedex, France
[3] GET-OMP, UMR 5563, 14, avenue Edouard Belin, 31400 Toulouse, France

Received: 23 June 2020 / Accepted: 22 March 2021 / Publishing online: 8 April 2021

Abstract – The Cenomanian to early Santonian interval is usually considered a time of postrifting tectonic quiescence around the northern margins of Iberia that preceded the onset of the Pyrenean convergence by crustal thrusting in the latest Santonian. However, plate kinematic models of the Mesozoic evolution of Iberia poorly constrain the Turonian-Santonian position of Iberia relative to Eurasia. This study reconstructs changes in the sedimentary facies and architecture of the Iberian carbonate platform throughout the Late Cretaceous and sheds new light on the geodynamic evolution of the Iberia-Eurasia relationship at that time. Sixteen outcrop sections were described and 24 sedimentary facies identified that define 5 depositional environments ranging from the deep marine basin to the continental setting. From these and previously published field data we reconstruct the evolution of the Pyrenean carbonate platform, on an east-west transect nearly 400 km long, on the basis of 11 short-term depositional sequences and 5 long-term hemicycles. In our interpretation, the Cenomanian and Turonian correspond to a postrift stage during which the European and Iberian margins, together with the deep basin between them, subside gently, as shown by accommodation rates varying from ~15 to 30 m/My in the margins and ~100 to 150 m/My in the basin. The Coniacian and early Santonian are characterized by a large-scale flexural response consisting of (1) uplift of the southern Iberian margin, with negative accommodation rates, karstified surfaces and paleosols, and (2) increasing subsidence rates in the basin and its edges (the northern Iberian margin and eastern Aquitaine platform), with accommodation rates several times greater than during the Turonian. We propose that far-field stress possibly related to the northeastward motion of Africa, and/or onset of shortening at the Iberia-Europe boundary in the central and eastern Pyrenees led to the incipient large-scale flexural deformation in the Pyrenean domain. The late Santonian and Campanian are an early orogenic stage marked by rapid subsidence throughout the Pyrenean domain, except at its western end. We evidence for the first time a pre-orogenic flexure at the Iberia-Europe plate boundary induced by regional plate reorganisation between Africa and Europe during the Coniacian and the early Santonian.

Keywords: carbonate platform / facies / sequence stratigraphy / tectonics / Pyrenees / Late Cretaceous

Résumé – Mouvements verticaux à grande échelle sur la plateforme carbonatée ibérique du Cénomanien au Santonien : un indicateur d'une contrainte compressive pré-orogénique au Coniacien. L'intervalle Cénomanien à Santonien inférieur est considéré autour de la marge nord-ibérique comme une quiescence tectonique post-rift qui précède le début de la convergence pyrénéenne au Santonien terminal, mis en évidence par le début de l'épaississement crustal. Cependant, les modèles de cinématique des plaques montrent de sérieuses incertitudes sur la reconstitution de la position de l'Ibérie par rapport à l'Eurasie du Turonien au Santonien. Cette étude reconstruit les changements de faciès et d'architecture sédimentaires de la plateforme carbonatée ibérique au cours du Crétacé supérieur et jette un nouvel éclairage sur l'évolution géodynamique à la limite Ibérie-Eurasie à cette époque. Seize coupes sédimentaires d'affleurements ont été étudiées. Les 24 faciès

*Corresponding author: s.andrieu@brgm.fr

sédimentaires identifiés se répartissent en 5 environnements de dépôt depuis le basin marin profond jusqu'au continent. À partir de ces nouvelles données et de données de terrain précédemment publiées, nous avons reconstruit l'évolution de la plateforme pyrénéenne le long d'une coupe SO-NE longue d'environ 400 km, sur la base de onze cycles de dépôt de court terme et cinq demi-cycles de long terme. D'après notre interprétation, l'intervalle Cénomanien à Turonien correspond à un stade postrift durant lequel les marges européenne et ibérique ainsi que le bassin entre elles subsident lentement, comme le montrent les taux d'accommodation variant entre 15 et 30 m/Ma pour les marges et 100 à 150 m/Ma pour le bassin. Le Coniacien enregistre une flexuration à grande échelle caractérisée par (1) un soulèvement de la marge ibérique sud, avec des taux d'accommodation négatifs, des surfaces karstifiées et des paléosols (~20 m/Ma) et (2) une forte subsidence du bassin et de ses bordures (plateformes nord ibérique et sud européenne), avec des taux d'accommodation plusieurs fois supérieurs à ceux du Turonien. Nous proposons qu'une contrainte compressive « far-field » possiblement due au déplacement vers le Nord-Est de l'Afrique, et/ou le début de la convergence entre l'Ibérie et l'Europe dans la partie centrale et orientale des Pyrénées a entraîné cette déformation flexurale subtile à grande échelle du domaine pyrénéen et ouest-ibérique au cours du Coniacien. Le Santonien supérieur et le Campanien correspondent au stade orogénique précoce, marqué par une forte subsidence à l'échelle du domaine pyrénéen, excepté dans sa partie ouest. Nous mettons en évidence pour la première fois une flexure pré-orogénique à la limite Ibérie-Europe, induite par la réorganisation régionale des plaques entre l'Afrique et l'Europe au cours du Coniacien et du début du Santonien.

Mots clés : plateforme carbonatée / faciès / stratigraphie séquentielle / tectonique / Pyrénées / Crétacé supérieur

1 Introduction

The Late Cretaceous tectonic history in the vicinity of the boundary between the Iberian and European plates is usually considered in terms of three stages: (1) an Albian to early Cenomanian rifting stage, leading to the hyperextension of continental crust and local exhumation of subcontinental mantle at the basin floor (Jammes *et al.*, 2009; Lagabrielle *et al.*, 2010; Masini *et al.*, 2014; Teixell *et al.*, 2016), (2) a mid-Cenomanian to mid-Santonian quiescent stage associated with postrift subsidence on both the north Iberian and south European margins, and (3) the onset of Pyrenean convergence at the end of the Santonian, based in particular on the earliest evidence of crustal thrusting (Puigdefàbregas and Souquet, 1986; Puigdefàbregas *et al.*, 1992; Olivet, 1996; Srivastava *et al.*, 2000; Rosenbaum *et al.*, 2002; Sibuet *et al.*, 2004; Jammes *et al.*, 2009; Handy *et al.*, 2010; Vissers and Meijer, 2012; Mouthereau *et al.*, 2014; Macchiavelli *et al.*, 2017). Although the record of crustal thickening shows that convergence had already started at the end of the Santonian, this study sought to better constrain the age of the transition between the postrift stage and the onset of convergence.

Modeling the Mesozoic plate kinematic evolution of Iberia —based on seafloor magnetic anomalies, paleomagnetic studies and geophysical and geological data—has been the subject of increasing debate in recent decades (*e.g.*, Olivet, 1996; Vissers and Meijer, 2012; Neres *et al.*, 2013; Barnett-Moore *et al.*, 2016). Indeed, the interpretation of the magnetic anomalies along the West Iberia and Newfoundland continental margins used for plate kinematic reconstructions (*e.g.*, Sibuet *et al.*, 2004; Vissers and Meijer, 2012) has come under question (Bronner *et al.*, 2011). Moreover, recent work has highlighted the crucial limitations surrounding the Cretaceous paleomagnetic data from Iberia, including the low age resolution of sampling and the small number of sites and samples (Neres *et al.*, 2012, 2013; Barnett-Moore *et al.*, 2016). Paleomagnetic data for the Late Cretaceous are especially scarce and have high uncertainties, particularly for the early Late Cretaceous, from the Cenomanian to Santonian (Sibuet *et al.*, 2004; Neres *et al.*, 2012). The compilation of Neres *et al.* (2012) listed only 30 paleomagnetic poles for Iberia between 158 Ma (Oxfordian) and 68 Ma (Maastrichtian), and of these only the following 7 poles are from the Cenomanian to Santonian: 80 Ma (Campanian), 88 Ma (Coniacian), 90 Ma (Turonian-Coniacian boundary), 92 Ma (middle Turonian) and 94 Ma (Cenomanian-Turonian boundary). The single pole at 88 Ma represents the entire Coniacian-Santonian interval, raising questions as to the reliability and precision of proposed plate kinematic reconstructions of Iberia for this time period.

Geological field evidence for the earliest stage of Pyrenean compression is scarce. In Provence, syntectonic folding is known in the latest Santonian sedimentary series (Leleu, 2005; Leleu *et al.*, 2009). In the Sainte-Victoire System, an early stage of shortening occured during Campanian (Tempier and Durand, 1981; Espurt *et al.*, 2012), characterized by strike-slip faulting and syntectonic breccia deposits (Lacombe *et al.*, 1992). In the southern Pyrenees, Puigdefàbregas *et al.* (1992) suggested that the first Pyrenean thrusts developed as a result of the reactivation of Early Cretaceous normal faults during the late Santonian. Deep E-W elongated basins, parallel to the future Pyrenean belt, formed in front of these thrusts and filled with turbiditic deposits of late Santonian to Campanian age (Vallcarga Formation of Mey *et al.*, 1968) which are up to 6000 m thick in the north (Dubois and Seguin, 1978) and 2000 m thick in the south. In addition, the Sant Corneli and Turbon synsedimentary anticlines formed as a result of compression at the Campanian-Maastrichtian boundary (Papon, 1969; Simó, 1986).

Several studies in the Pyrenees have highlighted large changes in accommodation during the Late Cretaceous, especially during the Coniacian. Decreased accommodation on the Iberian platform is associated with the development of karstified surfaces (Booler and Tucker, 2002), erosive contacts (Boix *et al.*, 2011) and long-term sedimentary gaps (Drzewiecki and Simó, 2002). Increased accommodation is locally recorded in thin-skinned margins and basins, as in

Cotiella (López-Mir *et al.*, 2014, 2015), Saint-Jean-de-Luz (Razin, 1989) and the Corbières (Bilotte, 1985; Bilotte, 2007). These findings hint that the Turonian to early Santonian interval has a more complex tectonic history than usually considered.

From Cenomanian to Santonian time, a period of about 16 My (Ogg *et al.*, 2016), a vast carbonate platform developed on the Iberian margin in the future Southern Pyrenean and Axial Zones, bordering a deep rifted basin to the north (Vacherat *et al.*, 2017). The fossil record of foraminifers and rudists provides a reliable biostratigraphic framework to study the evolution of this platform. However, excepting the synthesis of Souquet (1967), biostratigraphic studies remain limited to specific areas or stages, such as the western Pyrenees around Saint-Jean-Pied-de-Port (Merle, 1974), the Axial Zone from Laruns to Gavarnie (Mirouse, 1962; Ternet, 1965; Al Hamawi, 1992), the south-central Pyrenees around Tremp (Simó, 1986, 1993; Drzewiecki and Simó, 1997, 2000, 2002; Vincens *et al.*, 1998; Booler and Tucker, 2002; Pomar *et al.*, 2005; Boix *et al.*, 2009, 2011), and the eastern Pyrenees around Montgri (Bilotte, 1985) (Fig. 1). This carbonate platform has tremendous potential for improving our understanding of the Cenomanian to Santonian evolution of the Iberian-European boundary because it offers a continuous biostratigraphic record of 16 My that has never been studied as a whole.

The first objective of this paper is to reconstruct the changes in facies, architecture, and accommodation of the Late Cretaceous Iberian carbonate platform to compute vertical movements and their spatial distribution. The second objective is to compare our results with other sedimentary records from the inherited rift basin and the Aquitaine platform to improve our understanding of the sedimentary record and geodynamic activity of the greater Iberian-European boundary during this period.

2 Geological setting

The Pyrenean mountain belt is a N110° trending orogenic system that extends more than 400 km from the Bay of Biscay in northern Spain to the Mediterranean Sea in southern France (Fig. 1A). Five tectonostratigraphic zones are identified in the orogen, from north to south: the foreland Aquitaine Basin, the North Pyrenean Zone, the Axial Zone, the South Pyrenean Zone, and the foreland Ebro Basin (Fig. 1B). The Ebro Basin and South Pyrenean Zone are on the Iberia plate and are separated by the South Pyrenean Frontal Thrust (Fig. 1B; Vergés *et al.*, 1995, 1998) and contain mainly Mesozoic to Cenozoic sediments. The Axial Zone, in the core of the Pyrenean orogen, is bounded to the north by the North Pyrenean Fault (Fig. 1B). It consists mainly of Paleozoic basement rocks with Mesozoic sediments on its flanks (Muñoz, 1992, and references therein). The North Pyrenean Zone represents the inverted Early Cretaceous Iberia-Eurasia plate boundary that was in the deepest part of a hyperextended rift (*e.g.*, Mouthereau *et al.*, 2014; Teixell *et al.*, 2016; Espurt *et al.*, 2019; Lagabrielle *et al.*, 2020; Saspiturry *et al.*, 2020a, 2020b, 2021), and the Aquitaine Basin represents an inverted Early Cretaceous continental rift on the European proximal margin (*e.g.*, Angrand *et al.*, 2018; Issautier *et al.*, 2020). The North Pyrenean Frontal Thrust separates the Aquitaine Basin and the North Pyrenean Zone (Biteau *et al.*, 2006; Souquet *et al.*, 1977). The study area of this paper is a transect approximately 400 km long extending from Saint-Jean-Pied-de-Port in the western Pyrenees to Torroella de Montgri in the east (Fig. 1). The studied outcrops are located on the Iberia plate, south of the axis of the Pyrenean orogen, in the Axial Zone (outcrop sites 1–13) and the South Pyrenean Zone (sites 14–21, Fig. 1B).

From Cenomanian to Santonian time, the study area lay at subtropical latitudes (25°N) and was covered by a shallow epicontinental sea bordering a deep basin to the north (Vacherat *et al.*, 2017) (Fig. 2). Shallow marine carbonates were deposited upon a vast platform open to the Atlantic Ocean to the west and the Alpine Tethys to the east (Philip *et al.*, 2000).

Based on the work of Porthault (1974), Bilotte (1984, 1985), and Boix *et al.* (2009, 2011) on foraminifer, rudist and chlorophyte faunas, we compiled a precise and reliable biostratigraphic framework at the substage scale for the Cenomanian to Santonian deposits of the Pyrenees that is tied to the global reference geologic time scale (Ogg *et al.*, 2016; Fig. 3). Foraminiferal studies of Upper Cretaceous outcrops, beginning with the pioneering work of Souquet (1967) at the Pyrenean scale, have refined the faunal record in areas around Torroella de Montgri (Bilotte, 1984, 1985), Tremp (Caus and Cornella, 1983; Boix *et al.*, 2011), Laruns (Ternet, 1965; Al Hamawi, 1992; Ternet *et al.*, 2004), Saint-Jean-Pied-de-Port (Casteras, 1971; Merle, 1974; Le Pochat *et al.*, 1978) and Canfranc (Aragüés *et al.*, 1989; Teixell *et al.*, 1994). These have made it possible to propose reliable stage and substage attributions for the stratigraphic formations in our study area. From this information, in turn, we have compiled a schematic lithostratigraphic correlation diagram for the transect in Figure 4.

The oldest Late Cretaceous sediments in the study area date from the middle Cenomanian. They rest unconformably upon the Paleozoic basement, where parts of the Mesozoic sedimentary cover were displaced northward and eroded during the Albian-Cenomanian rifting stage (Saspiturry *et al.*, 2019a). The Saint-Jean-Pied-de-Port area (Fig. 4) features shallow lagoonal to barrier carbonates containing rudists and corals, that are dated as middle to late Cenomanian by their foraminifer content (Calcaires à préalvéolines member, Calcaires des cañons Formation, dated by *Praealveolina cretacea*, *Ovalveolina ovum* and *Chrysalidina gradata*; Merle, 1974; Le Pochat *et al.*, 1978). These shallow platform facies pass laterally to the Calcaire lité member around Laruns (Fig. 4), where they consist of clayey dark mudstone with rare bivalves and benthic foraminifers (*Praealveolina cretacea*; Calcaires des cañons Formation; Ternet, 1965). In the South Pyrenean Zone and eastern part of the Axial Zone, a vast lagoon developed during the middle and late Cenomanian (Santa Fé Formation; Bilotte, 1985; Simó, 1986; Drzewiecki and Simó, 1997, 2000, 2002; Booler and Tucker, 2002; Boix *et al.*, 2011), dated by benthic foraminifers (*Praealveolina cretacea*, *Ovalveolina ovum*; Souquet, 1967). In the subsiding Sopeira minibasin (Ribagorça salt basin), to the north of the Tremp basin, a thick series of marl and slope breccia formed consequent to the development of the Aulet diapir (Fig. 1; Saura *et al.*, 2016).

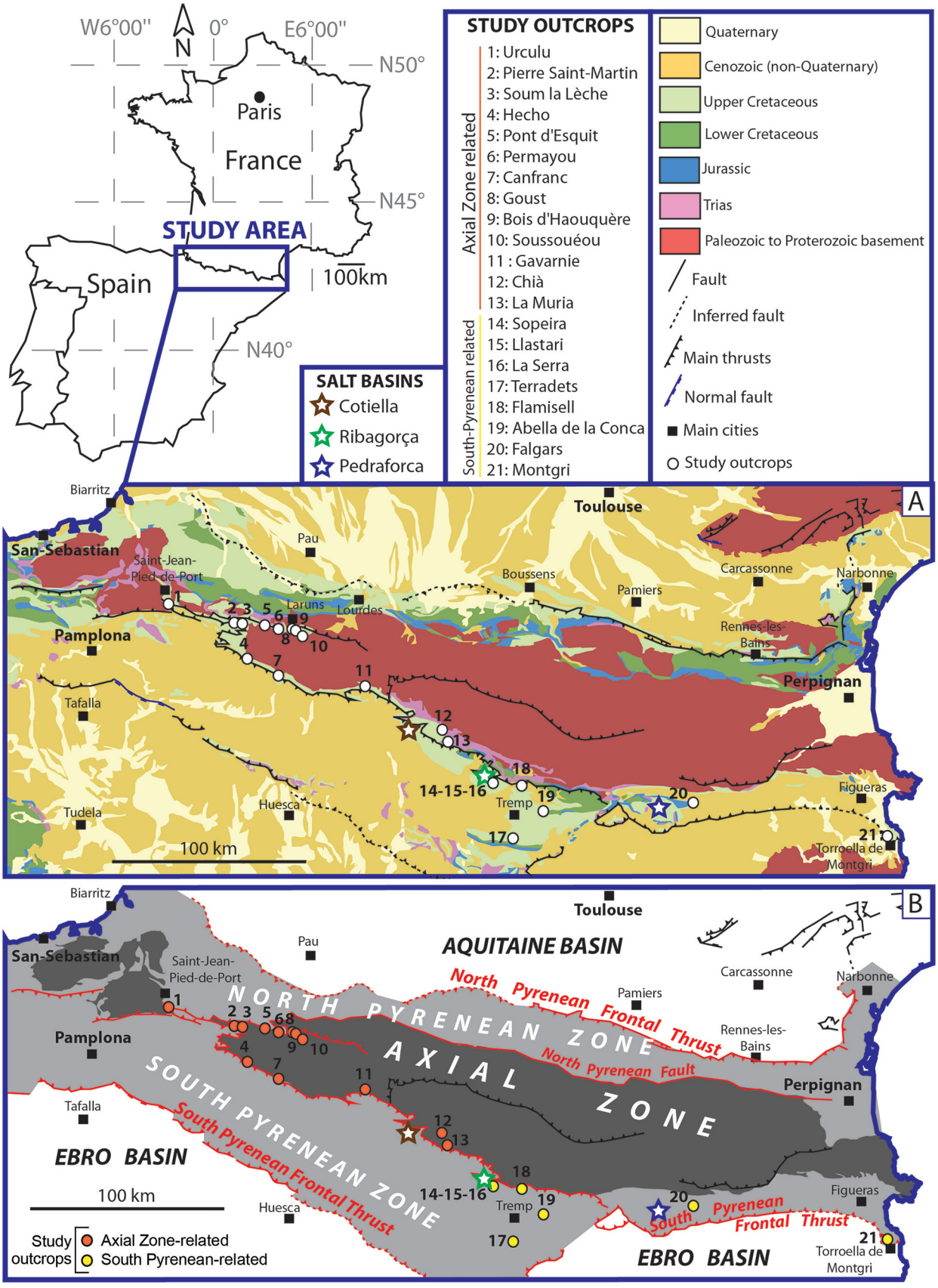

Fig. 1. A. Simplified geological map of the Pyrenees showing locations of the study outcrops and major faults. B. Major geologic provinces and faults of the Pyrenees (modified from Teixell, 1996; Clerc *et al.*, 2016).

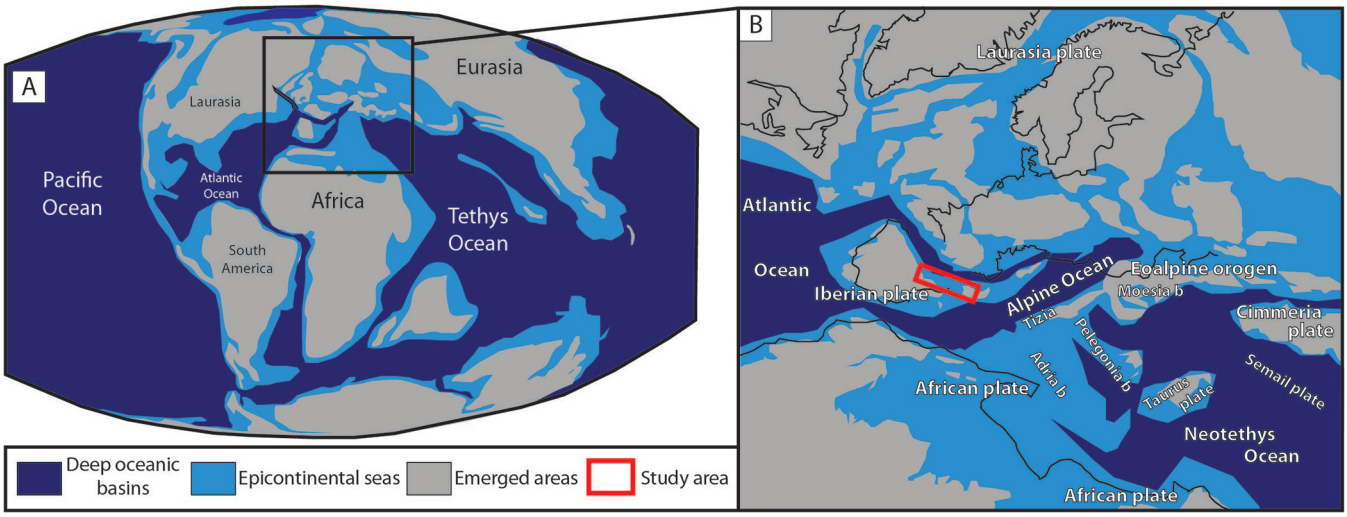

Fig. 2. A. Global paleogeographic map during the Albian-Cenomanian transition (100 Ma) (simplified from map by R. Blakey at http://cpgeosystems.com). B. Detail of A showing the location of the study area in the Western Tethys.

During the Turonian, no major paleogeographical changes occurred in the western part of the Axial Zone (Fig. 4). Shallow bioclastic limestone formed around Saint-Jean-Pied-de-Port (Calcaire graveleux member, Calcaires des cañons Formation), passing toward Laruns to open-marine dark limestone with very rare fauna (the chlorophyte *Halimeda elliotti*; Calcaire massif member, Calcaires des cañons Formation; Al Hamawi, 1992). Open-marine carbonates with abundant planktonic foraminifers and rare benthic foraminifers extend eastward from Tremp to Torroella de Montgri (Pardina Limestones; *Vidalina hispanica*; Souquet, 1967; Simó, 1993).

The Coniacian was a time of major paleogeographical reorganization in the study area, especially in the western part of the Axial Zone (Fig. 4). Around Saint-Jean-Pied-de-Port, shallow bioclastic limestone disappears in favor of open-marine glauconitic wackestone with planktonic foraminifers (Calcaires schisteux member, Calcaires des cañons Formation; *Marginotruncana sigali*, *M. renzi*, *M. pseudolinneiana*, *M. coronate*, *M. differens*, *M. imbricate*, *Hedbergella planispira*; Le Pochat *et al.*, 1978). This changes laterally to dolomitized limestone towards Laruns (Calcaire dolomitique member, Calcaire des cañons Formation; Al Hamawi, 1992; Ternet *et al.*, 2004). Shallow-marine shoal to lagoonal carbonates predominate both in the South Pyrenean Zone from Tremp (Congost and Montagut limestones; Skelton *et al.*, 2003) to Montsec (La Cova limestones; *Pseudolacazina loeblichi*, *Lacazina pyrenaica*; Boix *et al.*, 2011) and in the eastern part of the Axial Zone (Torroella de Montgri; Bilotte, 1985). At this time an exposure surface extended from Tremp to Torroella de Montgri, sometimes associated with a sedimentary gap, above shallow carbonate facies (Fig. 4; Simó, 1986; Booler and Tucker, 2002). In the Tremp area, the depositional profile deepens northward with the deposit of outer ramp marls (Reguard and Anserola marls, Fig. 4). The Cotiella and Ribagorça salt basins (Sant Gervás minibasin) record a sharp increase in subsidence rates related to the development of north-dipping thin-skinned detachment faults rooted in Triassic salt deposits (López-Mir *et al.*, 2014, 2015; Saura *et al.*, 2016).

Deeper water prevailed in the study area during the Santonian. Around Saint-Jean-Pied-de-Port, fine glauconitic and clayey limestones were deposited, dated from the planktonic foraminifers *Marginotruncana coronata*, *M. angusticarinata*, *M. concavata*, *M. pseudolinneiana* and *Nummofallotia cretacea* (Calcschistes verts and Calcaire à silex members, Calcaires des cañons Formation; Le Pochat *et al.*, 1978). To the east near Laruns, quartz-rich granular limestone (Calcaire gréseux member, Calcaires des cañons Formation; *Nummofallotia cretacea*; Ternet, 1965) gives way vertically to muddy bioclastic limestone (Calcaire bioclastique and Calcaire à silex members, Calcaires des cañons Formation; *Lacazina elongata*, *Nummofallotia cretacea*, *Orbitoides tissoti*; Casteras, 1971). In the South Pyrenean Zone and the eastern part of the Axial Zone, shallow lagoonal facies of the Coniacian to early Santonian are overlain by the Anserola Marls (Tremp and Torroella de Montgri areas; *Nummofallotia cretacea*; Bilotte, 1985) and the Font de les Bagasses Marls (Montsec area; foraminifers including *Lacazina elongata*; Hottinger, 1966; Caus and Cornella, 1983; Caus and Gómez-Garrido, 1989; Boix *et al.*, 2011). In the western part of the Axial Zone, the Anserola Marls are succeeded by the Castell de Montgri Formation, consisting of granular rudist and peloid limestones (middle to late Santonian; *Lacazina compressa*, *Periculina zitteli*; Bilotte, 1985).

3 Material and methods

3.1 Sedimentology

This study is based on the detailed examination of 16 outcrop sections along a 400-km transect between the cities of Saint-Jean-Pied-de-Port and Torroella de Montgri (Urculu, Pierre Saint-Martin, Soum la Lèche, Hecho, Pont d'Esquit, Permayou, Canfranc, Goust, Bois d'Haouquère, Soussouéou, Gavarnie, Terradets, Flamisell, Abella de la Conca, Falgars and Montgri; sites 1–11 and 17–21 in Fig. 1, respectively), supplemented by previous descriptions of 5 outcrop sections:

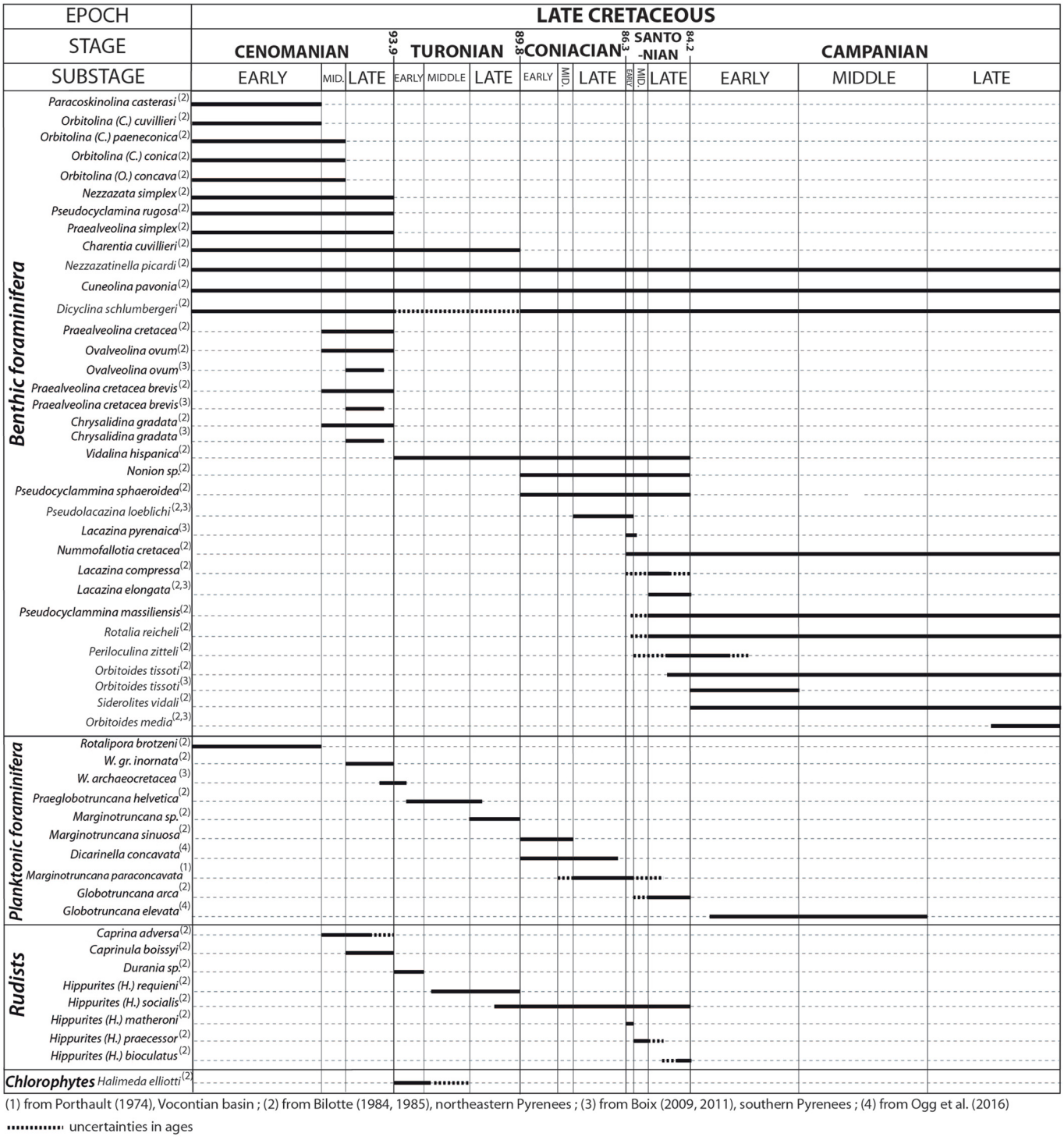

Fig. 3. Time distribution of benthic and planktonic foraminifer, rudist and chlorophyte fauna from Cenomanian to Campanian time.

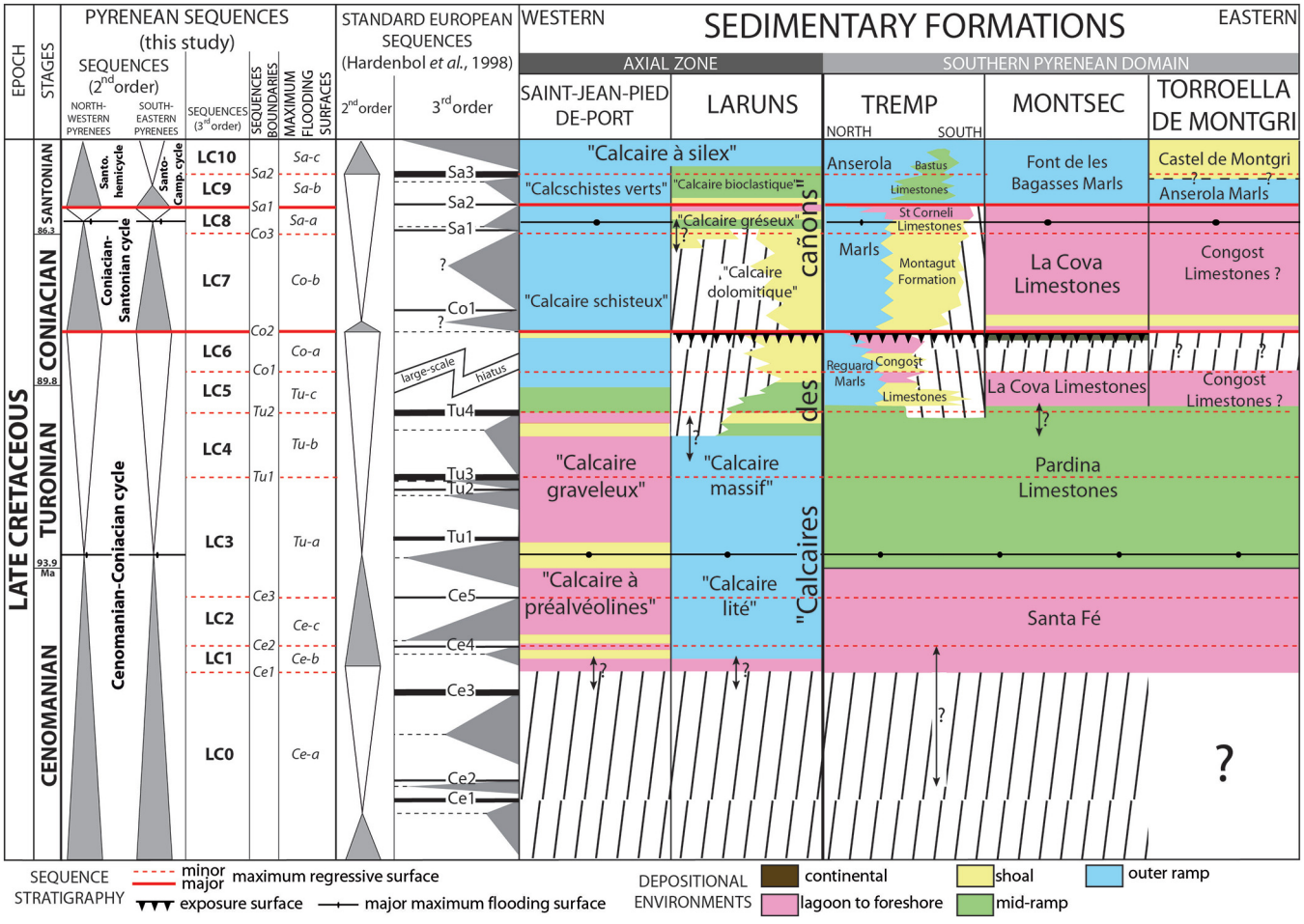

Fig. 4. Schematic lithostratigraphic diagram of the study area transect. Saint-Jean-Pied-de-Port area from Le Pochat *et al.* (1978), Laruns area from Ternet *et al.* (2004), Tremp area from Booler and Tucker (2002) and Skelton *et al.* (2003), Montsec area from Boix *et al.* (2011) and Torroella de Montgri area from Bilotte (1985). Stage boundary ages from Ogg *et al.* (2016) and standard European sequences from Hardenbol *et al.* (1998).

Chià and La Muria (sites 12 and 13; Souquet, 1967) and Sopeira, Llastari and La Serra (sites 14–16; Drzewiecki and Simó, 2002) (Fig. 1). The outcrop sections were logged in detail, characterizing their lithology, texture, allochem content, and sedimentary structures. Facies were determined on the basis of visual characterization of components (skeletal and non-skeletal grains), textures, sedimentary structures, sorting, and grain size in 130 thin sections. For each facies, paleodepths were estimated on the basis of sedimentary structures, textures, and allochems. The classic wave zonation was used, assuming depths of 10–15 m for the fair-weather wave base (Sahagian *et al.*, 1996; Plint, 2010). The standard facies zones of the Burchette and Wright (1992) model for homoclinal carbonate ramps, modified by Flügel (2010, p. 666), were used for depositional environment subdivisions and interpretations on the platform. The slope to basin area was divided into slope, toe of slope and basin depositional environments.

3.2 Sequence stratigraphy

Outcrop sections were interpreted in terms of sequence stratigraphy as defined by Embry (2009) to establish a stratigraphic cross-section. In this sequence stratigraphy model, units are bounded either by a subaerial unconformity when the surface was exposed or by a maximum regressive surface when the surface was not exposed. Subaerial unconformities or maximum regressive surfaces form sequence boundaries *sensu* (Embry, 2009). Depositional sequences within these boundaries are composed of transgressive and regressive systems tracts. As noted by Catuneanu *et al.* (2011), the surfaces that are selected as sequence boundaries vary among practitioners of sequence stratigraphy and are typically a function of which surfaces are best expressed within the context of each locality. Embry's model is particularly well suited to our study area because maximum regressive surfaces and subaerial unconformities are well expressed from the foreshore to offshore settings. We did not differentiate highstand system tracts from lowstand system tracts, classifying both as regressive system tracts (Embry, 2009; Catuneanu *et al.*, 2011).

3.3 Decompacted depth and accommodation calculations

Decompacted depth, also called total subsidence, corresponds to the thickness of sediments after decompaction

(Steckler and Watts, 1978; Allen and Allen, 2005). Goldhammer (1997) demonstrated that, in mud-supported carbonates at least, most compaction occurs during shallow burial with 100 to 400 m overburden. Considering that all of the Cenomanian to Santonian strata in this study were buried beneath more than 500 m of sedimentary deposits, we adopted uniform compaction factors of 1.2 for grainstones, 1.5 for packstones, 2 for wackestones, 2.5 for mudstones, and 3 for marls (Hillgärtner and Strasser, 2003).

Accommodation can be defined as the sum of the decompacted thickness of sediments and paleodepth variations (Robin *et al.*, 2000). Paleodepths for each facies were estimated on the basis of sedimentary structures and fossil fauna. We used the classic wave zonation, assuming depths of 10–15 m for the fair-weather wave base and more than 40 m for the storm wave base (Sahagian *et al.*, 1996; Plint, 2010).

Decompacted sediment thickness and accommodation values were calculated for short-term sequence tops, corresponding to maximum regressive surfaces, to reconstruct the evolution of sequences from Cenomanian to Santonian time.

Uncertainties in accommodation may be due to uncertainties in (1) the estimated sediment thickness, (2) the chosen compaction law and (3) the estimated paleodepth. We chose to assign an uncertainty of 5% to sediment thickness estimates. Uncertainties in decompaction factor estimates depend on the chosen compaction law (Goldhammer, 1997; Hillgärtner and Strasser, 2003); we estimated an uncertainty of 20% from the compaction law of Goldhammer (1997). Paleodepth estimates ranged from 50 m to more than 100 m for the lower offshore, 30 m ± 10 m for the upper offshore, 10 m ± 5 m for the shoreface, 5 m ± 5 m for the lagoon. Paleoelevations estimates ranged from 0 m to 25 m above sea level for continental environments. Nevertheless, there is no conclusive field evidence to determine a maximum value for paleoelevations. A depth of at least 75 m was assumed for lower offshore environments. In the basin (turbidite facies), only decompacted sedimentation rates were considered given that changes in paleobathymetry cannot be determined precisely at these depths.

4 Results

4.1 Sedimentary facies

We identified 24 different facies in the sedimentary rocks of our transect. The facies were grouped into five positions within the downdip profile: the slope to basin for facies deposited in deep marine environments (facies group F1, two facies), the outer ramp for facies deposited below the storm wave base on the platform (F2, four facies), the mid-ramp for facies deposited between the storm wave base and the fair-weather wave base (F3, five facies), the shoal/barrier environments in the inner ramp for wave- and tide-dominated facies deposited above the fair-weather wave base (F4, six facies), and lagoon to continental environments for facies deposited in calm and shallow environments, or continental environments above high tides (F5, seven facies). Observations and descriptions are summarized in Table 1 and presented in detail below.

4.1.1 Slope to basin: facies F1a and F1b

Description — Facies F1a (Fig. 5A) consists of alternating beds of fine sediment (clay to mudstone) and sandstone to detrital limestone. Facies F1b is a very coarse polygenic carbonate breccia with pebble to boulder-sized clasts as large as several meters (Fig. 5B).

Paleoenvironmental interpretation — In facies F1a, the alternations of fine and coarse sediment in normally graded sequences are characteristic of turbidites deposited in deep basins. Shallow fauna such as corals or benthic foraminifers are exported from the platform. In facies F1b, the very coarse clasts from various origins (shallow carbonate platform to Paleozoic basement) and the presence of erosive basal surfaces and slumps indicate high-energy deposits derived from the platform on the lower part of a steep slope (Drzewiecki and Simó, 2002). The study of facies and lateral facies variations indicates that facies F1b is located along the slope or at toe of slope (Drzewiecki and Simó, 2002).

4.1.2 Outer ramp: facies F2a to F2d

Description — These facies are claystones (F2a), marls (F2b), marls alternating with micritic limestone (F2c, Fig. 5C) and clayey glauconitic-planktonic mudstones (F2d, Fig. 5D).

Paleoenvironmental interpretation — The very fine grain size, absence of sedimentary structures, abundant bioturbation, and presence of abundant planktonic foraminifers, glauconite and clay indicate a very calm depositional environment, probably below the storm wave base in an outer ramp domain.

4.1.3 Mid-ramp: facies F3a to F3e

Description — Five facies were identified: calcisphere-planktonic foraminiferal wackestones (F3a, Fig. 5E), echinoderm wackestone to packstone (F3b), bivalve wackestone to packstone (F3c, Fig. 5F), coral fragment wackestone to packstone (F3d, Fig. 5G) and bioclastic quartz-rich wackestone to packstone (F3e, Fig. 5H). Thin marl interbeds are sometimes intercalated within these bioclastic facies.

Paleoenvironmental interpretation — The dominant fauna and common bioturbation indicate normal oxygenation and salinity conditions. The accumulation of fragmented bivalve shells forming shell-graded layers (F3c and F3d), gutter casts (F3a–d), hummocky cross-stratification (HCS, F3b–e), and wave ripples (F3c and F3d) suggests that sedimentation was under storm influence in the mid-ramp between the storm wave base and the fair-weather wave base.

4.1.4 Shoals/barriers in the inner ramp: facies F4a to F4f

Description — Six facies were identified: bioclastic peloidal grainstone (F4a, Fig.6A, B), foraminiferal grainstone (F4b, Fig. 6C), intraclast-lump grainstone to rudstone (F4c, Fig. 6D), coral build-ups in peloidal grainstones (F4d), quartz-bioclastic grainstones (F4e, Fig. 6E, G and H), and quartz sandstones (F4f, Fig. 6F). Microbial peloids are present in varying amounts (F4a and F4b).

Paleoenvironmental interpretation — The presence of grainstone to boundstone textures, wave ripples (Fig. 6B), tabular to trough cross bedding in dunes (Fig. 6G–H), *Thalassinoides* bioturbations, flaser to wavy bedding suggests a high-energy wave- or tide-influenced environment above the fair-weather wave base. Tide-dominated facies correspond to facies F4e and F4f, which display bidirectional tangential cross-bedding in plurimetric dunes, flaser to wavy bedding and

Table 1. Lithology, sedimentary structure and paleoenvironmental interpretations of Cenomanian to Santonian rocks of the Iberian margin of the Pyrenees.

Position within the downdip profile (hydrodynamism)	Lithofacies	Non-bioclastic components	Bioclastic components	Sedimentary and biogenic structures	Sorting and grain size	Energy and depositional environment
Slope to basin	F1a: turbidites	Quartz (C), glauconite (R), micas (R), peloids (R)	Planktonic foraminifers (R), calcispheres (R), benthic foraminifers (R), bivalves (R), echinoderms (R), corals (R)	Alternating fine sediment (clay to mudstone) and sandstone to detrital limestone, planar bedding	Moderately sorted, <4 μm for clay and up centimetric elements for sandstones, normally graded sequences	Basin (lower offshore)
	F1b: carbonate breccia	Rock clasts with various lithology: Cretaceous carbonate platform (foraminiferal mudstone to peloidal grainstone), Paleozoic basement	Planktonic foraminifers (R), calcispheres (R)	Erosive basal surfaces, slumps, matrix to clast supported	Poorly sorted, pluricentimetric to plurimetric clasts	Slope (lower offshore)
Outer ramp	F2a: claystone	Silt (R)	Planktonic foraminifers (R), benthic foraminifers (R), bivalves (R), echinoderms (R)	Abundant bioturbation	Very well sorted; <4 μm	Very low energy, lower offshore
	F2b: marl	Silt (C)	Planktonic foraminifers (R), benthic foraminifers (R), bivalves (R), echinoderms (R)	Abundant bioturbation	Very well sorted	Very low energy, lower offshore
	F2c: alternating marl and micritic limestone	Glauconite (R), oxides	Planktonic foraminifers (R), benthic foraminifers (R), bivalves (R)	Abundant bioturbation	Very well sorted	Very low energy, lower offshore
	F2d: clayey glauconitic-planktonic foraminiferal mudstone	Glauconite (R), ferruginous peloids (R), quartz (R), micas (R)	Planktonic foraminifers (R), benthic foraminifers (R), echinoids (R), crinoids (R), bivalves (R), brachiopods (R), green algae (R), dinoflagellates (R)	Bioturbation	Well sorted, 50 μm to 5 cm	Low energy, lower offshore
Mid-ramp	F3a: calcisphere-planktonic foraminiferal wackestone	Lumps (R), glauconite (R)	Calcispheres (A), planktonic foraminifers (C), bivalves (C), crinoids (C), echinoids (R)	Bioturbation, wave ripples, gutter casts	Well sorted, 20–500 μm	Low to moderate energy, upper offshore
	F3b: echinoderm wackestone to packstone	Peloids (R), quartz (R)	Crinoids (A), echinoids (F), bivalves (C), bryozoans (C), benthic foraminifers (R), gastropods (R), miliolids (R)	Bioturbation, gutter casts, hummocky cross-stratification (HCS)	Moderately sorted, 200 μm to 3 cm	Low to moderate energy, upper offshore
	F3c: bivalve wackestone to packstone		Bivalves (A), crinoids (C), corals (C), rudists (R), echinoids (R), bryozoans (R), gastropods (R), benthic foraminifers (R), planktonic foraminifers (R)	Bioturbation, shell-graded layers, wave ripples, gutter casts	Moderately sorted, 50 μm to 5 cm	Low to moderate energy, upper offshore

Table 1. (continued).

Position within the downdip profile (hydrodynamism)	Lithofacies	Non-bioclastic components	Bioclastic components	Sedimentary and biogenic structures	Sorting and grain size	Energy and depositional environment
	F3d: coral fragments wackestone to packstone	Peloids (C), intraclast (R), quartz (R)	Corals (A), bivalves (C), benthic foraminifers (C), crinoids (R), echinoids (R)	Bioturbation, shell-graded layers, wave ripples, gutter casts	Poorly sorted, 50 μm to 10 cm	Low to moderate energy, upper offshore
	F3e: bioclastic quartz-rich wackestone to packstone	Quartz (A), peloids (R)	Bivalves (C), crinoids (C), echinoids (R), bryozoans (R), corals (R), miliolids (R)	Bioturbation, hummocky cross-stratification (HCS)	Moderately sorted, 50 μm to 3 cm	Low to moderate energy, upper offshore
	F4a: bioclastic peloidal grainstone	Peloids (A), superficial ooids (R), intraclasts (R), quartz (R)	Crinoids (F), bryozoans (C), bivalves (R), echinoids (R), corals (R), gastropods (R), miliolids (R), *Prealveolina* (R), serpulites (R)	Unidirectional cross-bedding in megaripples, microbial peloids, wave ripples	Moderately sorted, 100 μm to 3 cm	High energy wave-dominated shoreface
	F4b: foraminiferal grainstone	Peloids (F), superficial ooids (R), intraclasts (R)	Miliolids (F), other benthic foraminifers (F), *Prealveolina* (R), bivalves (R), echinoderms (R)	Cross-bedding in megaripples, microbial peloids	Well sorted, 50–300 μm	High energy wave- to tide-dominated shoreface
	F4c: intraclasts-lump grainstone to rudstone	Intraclasts (F), lumps (C), peloids (R), quartz (R)	Bryozoans (C), bivalves (C), crinoids (C), echinoids (C), corals (C), gastropods (R), red algae (R)		Poorly sorted, 100 μm to 5 cm	High energy wave- to tide-dominated shoreface
Shoals/barrier in the inner ramp	F4d: coral bioconstructions (mixstone) in peloidal grainstones		Branching coral, lamellar corals, massive corals (A), bivalves (C), gastropods (C), bryozoans (R), echinoids (R), crinoids (R)	Bioherms and biostromes		High energy wave- to tide-dominated shoreface
	F4e: quartz-bioclastic grainstone	Quartz (F), peloids (C), intraclasts (R), superficial ooids (R)	Bivalves (C), crinoids (C), echinoids (R), corals (R), bryozoans (R), miliolids (R), *Prealveolina* (R), other benthic foraminifers (R), brachiopods (R)	Bioturbations (*Thalassinoides*), bidirectional tangential cross-bedding in centimetric megaripples to plurimetric dunes, conjugate ripples, clay drapes	Moderately sorted, 100 μm to 3 cm	High energy tide-dominated shoreface
	F4f: quartz sandstone	Quartz (A), lithoclasts (C), feldspar (R), oxides (R), peloids (R)	Crinoids (R), bryozoans (R), bivalves (R), benthic foraminifers (R)	Bidirectional tangential cross-bedding in megaripples	Moderately sorted, 100 μm to 3 cm	High energy tide-dominated shoreface (estuarial environment)
	F5a: rudist micritic floatstone		Rudists (A), other bivalves (R), miliolids (R), other benthic foraminifers (R), gastropods (R), echinoderms (R)	Washover deposits, bioturbations	Poorly sorted, 50 μm to 20 cm	Moderate energy protected environment, lagoon
Lagoon to continental environments	F5b: coral wackestone to floatstone	Peloids (C)		Washover deposits, bioturbations	Poorly sorted, 50 μm to 20 cm	Low to moderate energy protected environment, lagoon

Table 1. (continued).

Position within the downdip profile (hydrodynamism)	Lithofacies	Non-bioclastic components	Bioclastic components	Sedimentary and biogenic structures	Sorting and grain size	Energy and depositional environment
			Corals (A), bivalves (R), gastropods (R), bryozoans (R), echinoderms (R)			
	F5c: foraminiferal wackestone to packstone	Peloids (R), quartz (R), intraclasts (R), lumps (R)	Miliolids (F), *Prealveolina* (C), other benthic foraminifers (F), bivalves (C), corals (R), gastropods (R), crinoids (R)	Birdseyes	Moderately sorted, 50 μm to 2 cm	Low to moderate energy protected environment, lagoon to beach
	F5d: Peloid grainstone	Peloids (A), quartz (C), superficial ooids (R), intraclasts (R), lumps (R)	Crinoids (C), echinoids (R), bivalves (R), benthic foraminifers (R), corals (R), bryozoans (R)	Planar bedding	Moderately sorted, 100 μm to 3 cm	High energy foreshore environment (tidal sand flat)
	F5e: sandstone alternating with siltstone to mudstone layers	Quartz (A), feldspar (R), biotite (R), oxides (R), peloids (R)	Bivalves (R), benthic foraminifers (R), bryozoans (R), echinoderms (R)	Planar bedding, clay drapes	Moderately sorted, <4 μm to 3 cm	High energy foreshore environment (tidal sand flat)
	F5f: conglomerate	Quartz (A), lithoclasts (F), feldspar (R), oxides (R), peloids (R)	Rudists (R), other bivalves (R), miliolids (R), *Prealveolina* (R), corals (R), bryozoans (R), echinoderms (R)	Bioturbations, normal grading, erosive basal surface	Poorly sorted, 100 μm to 10 cm	High energy foreshore to beach environment
	F5g: paleosol	Clay (F), silt (F), quartz (F), iron hydroxides (C)	*Characeae* gyrogonites (R), oysters (R)	Roots (rhizolites)	Very well sorted; <4 μm	Backshore to continental environment

R = rare: <10%; C = common: 10–20%; F = frequent: 20–40%; A = abundant: >40%.

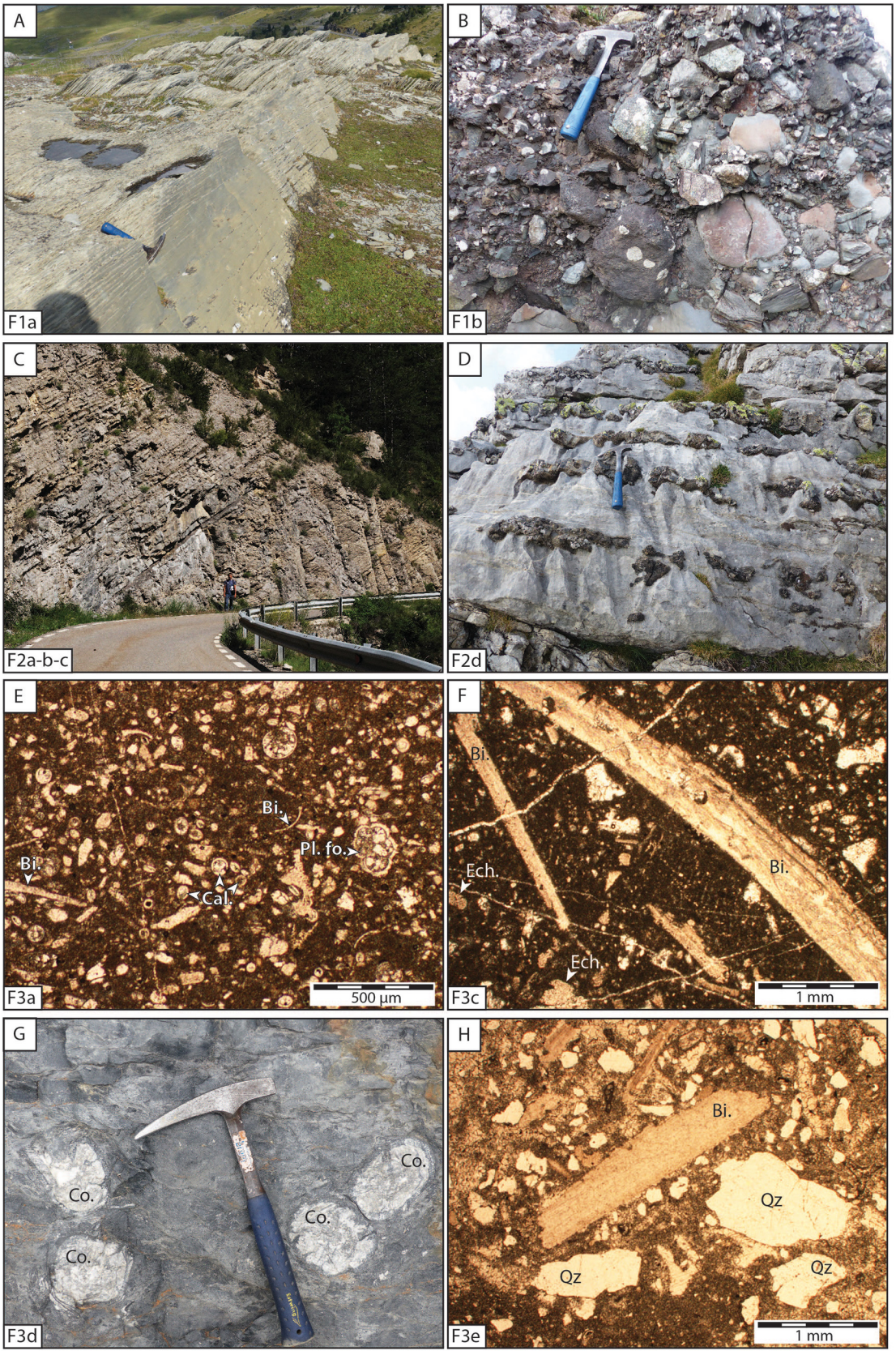
A
F1a
B
F1b
C
F2a-b-c
D
F2d
E
Bi.
Pl. fo.
Bi.
Cal.
F3a
500 µm
F
Bi.
Ech.
Bi.
Ech.
F3c
1 mm
G
Co.
Co.
Co.
Co.
F3d
H
Bi.
Qz
Qz
Qz
F3e
1 mm

are abundant in the western part of the Axial Zone in lower Santonian strata (Calcaire gréseux member, Calcaires des cañons Formation; Fig. 4). Facies F4a to F4d display cross-bedding in megaripples and wave ripples, indicating wave-dominated to locally tide-dominated environments. These facies, ubiquous in the study area, are characteristic of the Cenomanian to Coniacian interval.

4.1.5 Lagoon to continental environments: facies F5a to F5g

Description — Seven facies are distinguished: rudist micritic floatstone (F5a, Fig. 7A), coral wackestone to floatstone (F5b, Fig. 7B), foraminiferal wackestone to packstone (F5c, Fig. 7C), peloid grainstone (F5d, Fig. 7D), sandstone alternating with siltstone to mudstone layers (F5e, Fig. 7E, F), conglomerate (F5f, Fig. 7G, H) and paleosol (F5g).

Paleoenvironmental interpretation — The dominance of peloid facies, the abundance of miliolids and *Praealveolina* foraminifers argue for lagoonal to beach environments for facies F5a to F5d. In facies F5a and F5b, the presence of generally well-preserved gastropods and bivalves combined with local washover deposits is characteristic of a calm lagoon environment sporadically disturbed by events of high energy (probably storms). Birdseyes occurring in facies F5c are characteristic of the intertidal domain. Planar bedding, clay drapes and lamina-scale grains-size changes in facies F5d and F5e indicate variable hydrodynamic conditions in a tide-dominated flat. The very coarse grain size of facies F5f and the occurrence of erosive basal surfaces indicate high hydrodynamic conditions, probably in a foreshore to beach environment. In facies F5f, *Characeae* gyrogonites and roots indicate a backshore to continental environment.

4.2 Facies architecture and depositional sequences

Eleven transgressive–regressive cycles were identified between the early Cenomanian and the late Santonian (Fig. 4). Ten of these cycles are present on the shallow platform (LC1 to LC10, middle Cenomanian to late Santonian) and the remaining cycle is present in the basin (LC0, early to middle Cenomanian). Considering a time range of about 16 My for the entire interval (Ogg *et al.*, 2016), the average duration of a cycle is approximately 1.5 My, which is close to the duration of third-order cycles (Haq *et al.*, 1987; Hardenbol *et al.*, 1998; Schlager, 2004). These cycles are arranged into lower-order cycles (Fig. 4): a Cenomanian–Coniacian cycle topped by maximum regressive surface Co2, a Coniacian–Santonian cycle topped by maximum regressive surface Sa1, and a Santonian transgressive hemicycle.

Figure 8 is a correlation diagram for 16 outcrop sites along the length of the transect (sites 1–3, 5–13, 17–19 and 21 in Fig. 1). Figure 9 is a similar correlation diagram for a short north-south transect across the Iberian margin (sites 14–19 in Fig. 1). Figure 10 presents photographs of significant field features, and Figure 11 integrates our facies information and accommodation estimates in paleogeographic maps depicting four stages of transgression and regression during the Cenomanian–Santonian period.

4.2.1 Cenomanian transgressive hemicycle and early Turonian maximum flooding (sequences LC1 to LC3)

The Cenomanian to early Turonian includes four third-order sequences (LC0, LC1, LC2 and the transgressive systems tract of LC3) and is characterized by a second-order flooding trend ending at the early Turonian maximum flooding surface (Tu-a). Cenomanian sediments directly onlap the Paleozoic basement in the western part of the Axial Zone (Urculu, Permayou, Goust, Bois d'Haouquère, Soussouéou, Canfranc and Gavarnie sections; Figs. 8 and Figs. 8 and 10A, B) and overlie Albian sediments in the South Pyrenean Zone and the eastern part of the Axial Zone (La Muria, Sopeira, Llastari, La Serra, Terradets, Flamisell, Abella de la Conca and Montgri sections; Fig. 9). Where Cenomanian sediments directly overlie the Paleozoic basement, the lower part of the LC1 sequence is composed of transgressive polygenic conglomerates and sandstones (facies F5e and F5f).

In sequences LC1 and LC2, a wave-dominated carbonate rimmed platform extends the full length of the transect (Figs. 8, 9 and 11A). Lagoon sediments with retrograding geometries, rich in foraminifers and rudists (facies F5a and F5b), lie north of the study area in the Axial Zone in the Pays Basque (Urculu section) and south of the study area in the South Pyrenean Zone and the eastern part of the Axial Zone in Spain (Chià, La Muria, Terradets, Flamisell, Abella de la Conca, and Montgri sections). This lagoon is bordered by foraminiferal and peloidal shoals with rudists (facies F4a and F4b). The shoal facies pass northward into calcisphere–planktonic foraminiferal wackestones (facies F3a) that give way abruptly to basinal marls and breccias (facies F1). Maximum flooding surfaces in sequences LC1 and LC2 are marked by peloidal and foraminiferal shoal deposits within the lagoonal deposits.

Outer ramp environments are located to the north of the transect, especially in the sections described in this work from Laruns to Gavarnie in the Axial Zone (sites 2–11; Figs. 8, 9 and

Fig. 5. Photographs and thin section of basin, slope and mid-ramp facies. A. Calcareous flysch (facies F1a), La Pierre-Saint-Martin section, Calcschistes à Navarrelles Formation, sequence LC9. B. Polygenic clast-supported slope breccia (facies F1b) showing clasts with varying lithologies including Cretaceous carbonate platform (foraminifera mudstone to peloidal grainstone), Late Triassic magmatic rocks and Paleozoic metasediments, Brèche monumentale d'Errozaté Formation. C. Alternating marl and micritic limestone (facies F2a–c), Flamisell section, Reguard marls Formation, sequence LC5. D. Chert mudstone (facies F2d), La Pierre-Saint-Martin section, Calcaire à silex Formation, sequence LC9.E. Calcisphere (Cal)–planktonic foraminifera (Pl. Fo.) wackestone (facies F3a) with bivalves (Bi.), Urculu section, Calcaire schisteux Formation, sequence LC7. F. Bivalve wackestone (facies F3c) with echinoderms, Abella de la Conca section, Pardina Limestones Formation, sequence LC3. G. Coral (Co.) wackestone (facies F3d), Goust section, Calcaire massif member of the Calcaires des cañons Formation, sequence LC5. H. Quartz (Qz) and bivalve packstone (facies F3e), Soussouéou section, Calcaire lité member of the Calcaires des cañons Formation, sequence LC1.

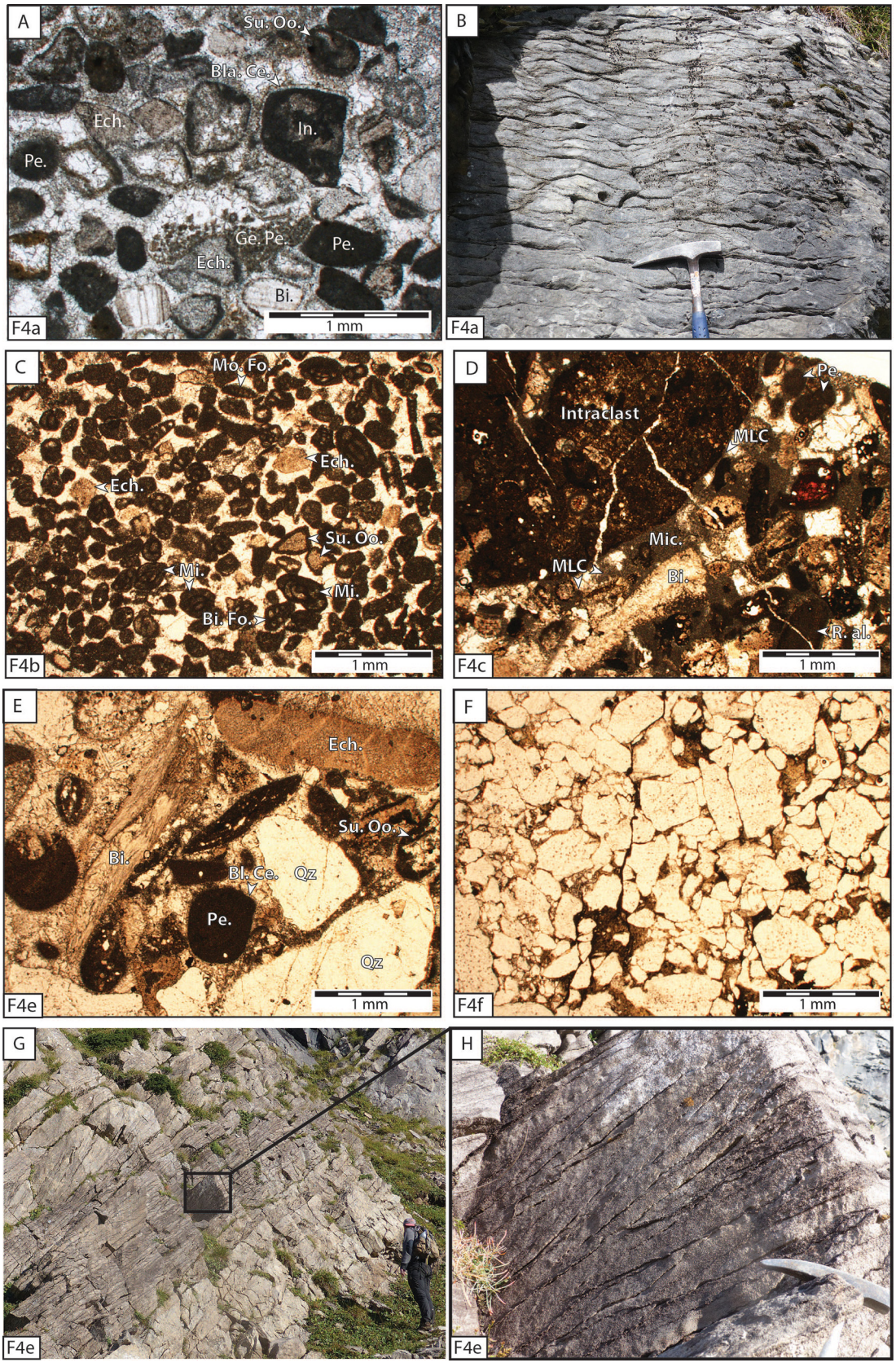
A
Su. Oo.
Bla. Ce.
Ech.
In.
Pe.
Ge. Pe.
Pe.
Ech.
Bi.
1 mm
F4a
B
F4a
C
Mo. Fo.
Ech.
Ech.
Su. Oo.
Mi.
Mi.
Bi. Fo.
1 mm
F4b
D
Pe.
Intraclast
MLC
Mic.
MLC
Bi.
R. al.
1 mm
F4c
E
Ech.
Su. Oo.
Bi.
Bl. Ce.
Qz
Pe.
Qz
1 mm
F4e
F
1 mm
F4f
G
F4e
H
F4e

11A). Facies correspond to claystones, marls, alternating marl and micritic limestone and clayey glauconitic mudstones (facies F2a–d). The maximum flooding surface Tu-a is marked by the presence of outer ramp to mid-ramp facies in the entire study area, except in the Urculu section, where it is characterized by the appearance of pluridecimetric foraminiferal grainstone within the lagoonal facies.

4.2.2 Turonian to Coniacian regressive hemicycle (sequences LC3 to LC6)

The Turonian to Coniacian regressive hemicycle is composed of four third-order sequences: the regressive systems tract of LC3 and sequences LC4, LC5 and LC6.

In the Turonian section (sequences LC3, LC4 and transgressive systems tract of sequence LC5), a deep ramp dips gently toward the north (Figs. 8, 9 and 11B). In the South Pyrenean Zone, the environments change northward from planktonic foraminiferal mid-ramp deposits (facies F3a) to clayey outer ramp deposits (facies F2a–d; Figs. 8 and 11B) and to basin deposits (facies F1b) in the Llastari and Sopeira sections (Figs. 9 and 11B). In the Saint-Jean-Pied-de-Port area, a shallow platform where lagoon environments are bordered by peloidal shoals and coral reefs (facies F4a, F4b, F4d and F5a–c) progrades eastward in the western Axial Zone (Urculu section).

In the Coniacian section (regressive systems tract of sequence LC5 and sequence LC6), the shallowing trend continues in the study area except in the Saint-Jean-Pied-de-Port area, which undergoes a sharp deepening (Figs. 8, 9 and 11C). A rudist and foraminiferal lagoon (facies F5a–c) appears in the eastern part of the study area in the South Pyrenean Zone and the eastern part of the Axial Zone (Terradets and Montgri sections) in the regressive systems tract of sequence LC5, whereas sequence LC6 is absent there. Coral reefs and bioclastic shoals (facies F4a–d) rim the lagoon, which is prograding northwestward (Chià, La Muria, Flamisell and Abella de la Conca sections). Sequences LC5 and LC6 are absent in the La Serra section but appear again in the basinal sediments of the Sopeira section (Fig. 9; Drzewiecki and Simó, 2002). In the western part of the Axial Zone (Goust to Gavarnie sections), mid-ramp to shoal environments are evident with bioclastic limestones (facies F3b–d and F4a–c), and siliciclastic limestones (facies F3e and F4e) lie to the south in the Canfranc section (Fig. 8). Deposits of sequences LC4 to LC6 are absent in the Permayou section area, either not deposited or eroded as a result of exposure. Farther west in the Axial Zone in the Saint-Jean-Pied-de-Port area (Urculu section), sequences LC5 to LC6 are marked by a retrograding trend with the occurrence of glauconitic and clayey mid to outer ramp limestones (facies F2b, F2c and F3a), unlike the rest of the study area (Figs. 8, 9 and 11C).

Sequence LC6 is topped by the major maximum regressive surface Co2. This discontinuity, described here from west to east, is associated with large-scale exposure in the Axial Zone and the South Pyrenean Zone (Figs. 8, 9 and 11C). In the Permayou section (Fig. 8), the Co2 surface is a subaerial unconformity where a massive beach conglomerate (facies F5f) of sequence LC7 directly overlies rocks of sequence LC3 (Fig. 10C, D), thus deposits of sequences LC4, LC5 and LC6 were either not deposited or removed by erosion. In the Goust and Bois d'Haouquère (Fig. 8) sections, the Co2 surface is a subaerial unconformity above foreshore beach carbonate facies (F5d). In the La Serra section (Fig. 9), the Co2 surface is directly on rocks of the LC4 sequence, the LC5 and LC6 cyles being absent (Drzewiecki and Simó, 2002). In the Terradets section it is associated with a paleosol horizon (facies F5g), and sequence LC6 is absent (Fig. 10F). In the Flamisell and Abella de la Conca sections (Fig. 9), the Co2 discontinuity represents a karstified surface (Booler and Tucker, 2002; Fig. 10E). Where the Co2 surface is not associated with exposure markers, it is at the top of bioclastic to siliciclastic shoal or lagoon facies (facies F4a–e, F5a, F5c and F5d).

4.2.3 Coniacian to Santonian cycle (sequences LC7 and LC8)

The Coniacian to Santonian cycle is composed of two third-order sequences: LC7 and LC8. During this time interval, shallow platform environments extended over the Iberian margin except around the Saint-Jean-Pied de-Port and Tremp areas (Fig. 8). Shallow platform environments correspond to lagoonal rudist and foraminifer wackestones to packstones (facies F5a, F5b and F5e) in the east (Terradets and Montgri sections) and west (Canfranc section), bioclastic to siliciclastic shoals (facies F4a–e) in the Tremp to Castejòn de Sos area (Chià and La Muria sections) and mid-ramp bioclastic to siliciclastic facies (facies F3b–e) in the Gavarnie and Laruns areas (Goust, Bois d'Haouquère, Soussouéou and Gavarnie sections). Tide-dominated depositional profiles are common in shallow platform environments of the Axial Zone: in the Laruns area, these include siliciclastic limestones and sandstones with metric crossbedded dunes (facies F4e and F4f), and around Torroella de Montgri they include tidal-flat peloid grainstones (facies F5c; Congost Limestones).

In the Saint-Jean-Pied-de-Port and Tremp areas (Fig. 8), sequences LC7 and LC8 display a sharp deepening with the

Fig. 6. Photographs and thin sections of shoal/barrier facies. A. Peloidal (Pe.) and bioclastic grainstone (facies F4a) with echinoderms (Ech.), bivalves (Bi.), intraclasts (In.), superficial ooids (Su. Oo.), geopetal peloidal fabrics (Ge. Pe.) and bladed cement (Bla. Ce.), Urculu section, Calcaire graveleux Formation, sequence LC3. B. Wave ripples in bioclastic limestone (facies F4a), Goust section, Calcaire dolomitique member of the Calcaire des cañons Formation, sequence LC7. C. Foraminifera (Fo.) grainstone (facies F4b) with monoserial foraminifera (Mo. Fo.), biserial foraminifera (Bi. Fo.), miliolids (Mi.), echinoderms and superficial ooids, Montgri section, Calcaire de Santa Fé Formation, Cenomanian-Coniacian cycle. D. Intraclast rudstone (facies F4c) with bivalves, red algae (R. al.), peloids, micritization (Mic.) and meniscus-like cements (MLC; Hillgärtner *et al.*, 2001), Terradets section, La Cova Formation, sequence LC7. E. Quartz (Qz) bioclastic grainstone (facies F4e) with bivalves, echinoderms, peloids, superficial ooids and bladed cement, Permayou section, Calcaire gréseux member of the Calcaires des cañons Formation, sequence LC7. F. Quartz sandstone (facies F4f), Bois d'Haouquère section, Calcaire lité member of the Calcaires des cañons Formation, sequence LC1. G and H. Cross-bedding in pluridecimetric dunes in quartz-bioclastic grainstone (facies F4e), Permayou section, Calcaire gréseux member of the Calcaires des cañons Formation, sequence LC7.

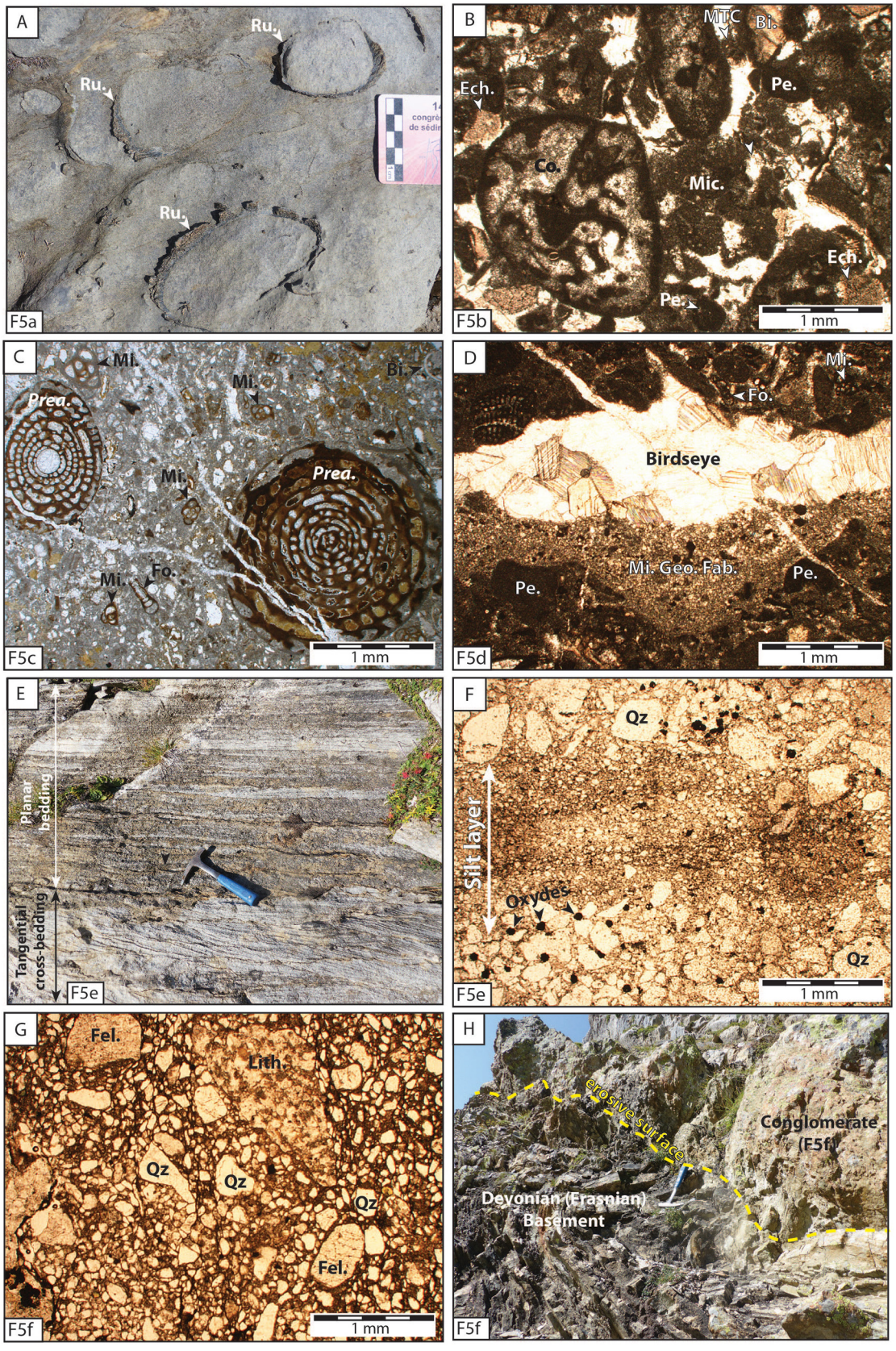
A
Ru.
Ru.
Ru.
F5a
B
MTC
Bi.
Ech.
Pe.
Co.
Mic.
Ech.
Pe.
1 mm
F5b
C
Mi.
Mi.
Bi.
Prea.
Mi.
Prea.
Mi.
Fo.
1 mm
F5c
D
Mi.
Fo.
Birdseye
Mi. Geo. Fab.
Pe.
Pe.
1 mm
F5d
E
Planar bedding
Tangential cross-bedding
F5e
F
Qz
Silt layer
Oxydes
Qz
1 mm
F5e
G
Fel.
Lith.
Qz
Qz
Qz
Fel.
1 mm
F5f
H
erosive surface
Conglomerate (F5f)
Devonian (Frasnian) Basement
F5f

appearance of outer platform marl and limestone-marl alternations (facies F2b–d) in the Urculu, Flamisell and Abella de la Conca sections and basin facies (facies F1) in the La Serra section (Fig. 9; Drzewiecki and Simó, 2002). Sequence LC8 is topped by the maximum regressive surface Sa1. This surface corresponds to an exposure discontinuity around Laruns, where it overlies tidal sand-flat sandstones with planar bedding and clay drapes (facies F5e) in the Permayou and Goust sections.

4.2.4 Santonian transgressive hemicycle (sequences LC9 and LC10)

The Santonian transgressive hemicycle is composed of two third-order sequences: LC9 and LC10. This time interval is characterized by retrograding architectures on the entire Iberian platform, where mid to outer ramp environments predominate (Figs. 8, 9 and 11D). In sequence LC9 inner platform environments persist locally in the western part of the Axial Zone, with rudist to *Praealveolina* lagoon facies (facies F5a-c) in the Soum la Lèche section (Fig. 8) and bio-siliciclastic shoal facies (facies F4a, F4b and F4e) in the Castejòn de Sos area in the Chià and La Muria sections. In the lower part of sequence LC10, the last remaining inner platform environments are flooded and progressively replaced by outer ramp environments with clayey limestones to marls facies (facies F2b–d) all over the Iberian margin. In the east in the Terradets and Montgri sections (South Pyrenean Zone), the regressive systems tract of sequence LC10 is topped by inner ramp and shoal deposits consisting of peloid to foraminifer shoal grainstones (facies F4a and F4b).

4.3 Decompacted sedimentation and accommodation in the Iberian platform

In Figure 12, we present reconstructions of the changes in decompacted sediment thickness and accommodation for each short-term sequence (LC1 to LC10) at eight key localities of the Iberian platform: Urculu, Canfranc, La Muria, Permayou, Gavarnie, Terradets, Flamisell and Montgri. These are summarized for each stage below and interpreted in terms of sedimentation and accommodation rates. Figure 11 shows the magnitudes and rates of sedimentation and accommodation for each locality.

The Cenomanian interval (sequences LC1 and LC2) is characterized by moderate sedimentation and accommodation rates on the Iberian margin. Sedimentation rates range from 1 m/My at Canfranc to 19 m/My in at La Muria, and accommodation rates range from 5 m/My at Montgri to 21 m/My at Gavarnie (Fig. 11A).

In the Turonian interval (sequences LC3, LC4 and transgressive systems tract of sequence LC5), sedimentation and accommodation rates increase over the whole Iberian margin. Sedimentation rates range from 13 m/My at Permayou to 81 m/My at Abella de la Conca, and accommodation rates range from 6 m/My at Canfranc to 98 m/My at Abella de la Conca (Fig. 11B).

In the Coniacian interval (regressive systems tract o sequence LC5 and sequences LC6 and LC7), sedimentation and accommodation rates show a significant decrease, except at Urculu (accommodation rate 52 m/My) and Flamisell (accommodation rate 160 m/My), where they increase suddenly associated with the appearance of outer platform environments (Fig. 11C). Accommodation rates are negative at Permayou, Canfranc, La Muria and Montgri (–21 m/My, −2 m/My, −2 m/My and −4 m/My, respectively); sedimentation and accommodation rates are 23 m/My and 16 m/My, respectively, at Terradets and 26 m/My and 13 m/My at Gavarnie. The LC6 sequence records the lowest values of decompacted sediment thickness and accommodation in the Coniacian section all over the Iberian platform; accommodation ranges from 63 m to −75 m in this sequence, with a mean value of 4 m (Fig. 12). In sequence LC7, accommodation values are high at Urculu (119 m) and Flamisell (585 m) and much lower (85 m to 0 m) at the other localities, yielding a mean value of 32 m (Fig. 12).

In the Santonian interval (sequences LC8, LC9 and LC10), sedimentation and accommodation rates significantly increase all over the study area. Sedimentation rates for this interval range from 77 m/My at Canfranc to 857 m/My at Flamisell, and accommodation rates range from 108 m/My at Canfranc to 857 m/My at Flamisell (Fig. 11D). The mean total accommodation is 195 m for sequence LC9, and accommodation values range from 34 m at La Muria to 600 m at Flamisell (Fig. 12). For sequence LC10, the mean total accommodation is 356 m, with values ranging from 76 m at Terradets to 658 m at Permayou (Fig. 12).

4.4 Synthesis of Pyrenean domain paleogeography and accommodation

4.4.1 Revised paleogeography of the Pyrenean domain

The results described above have enabled us to revise the paleogeographic reconstruction of Vacherat *et al.* (2017) by integrating structural constraints on the geometry of the

Fig. 7. Thin sections and photographs of lagoon and foreshore facies. A. Rudist (Ru.) micritic floatstone (facies F5e), Urculu section, Calcaire graveleux Formation, sequence LC3. B. Coral (Co.) grainstone (facies F5b) with peloids (Pe.), bivalves (Bi.) and echinoderms (Ech.), displaying meniscus types cements (MTC) and micritization (Mic.), Flamisell section, Congost Formation, sequence LC5. C. Wackestone (facies F5c) with *Praealveolina* (Prea.), miliolids (Mi.), undifferentiated foraminifera (Fo.) and bivalves (Bi.), Urculu section, Calcaire graveleux Formation, sequence LC1. D. Birdseye filled by microsparitic geopetal fabrics (Mi. Geo. Fab.) in a packstone (facies F5d) with miliolids, undifferentiated foraminifera and peloids, Canfranc section, Calcaire gréseux member of the Calcaires des cañons Formation, sequence LC7. E. Sandstone (facies F5e) with planar bedding, Permayou section, Calcaire gréseux member of the Calcaires des cañons Formation, sequence LC7. F. Thin silt layer with clay and quartz alternating with sandy quartz (Qz) layers (facies F5e), Soussouéou section, Conglomérat et grès de base member of the Calcaires des cañons Formation, sequence LC1. G. Quartz-rich conglomerate (facies F5f) with a clayey matrix, displaying lithoclasts (Lith.) and feldspar (Fel.), Permayou section, Conglomérat et grès de base member of the Calcaires des cañons Formation, sequence LC1. H. Polygenic conglomerate (facies F5f) with quartz (Qz) and Paleozoic lithoclasts (Li.) eroding Devonian basement, Permayou section, basal conglomerate of the Calcaires des cañons Formation, sequence LC1.

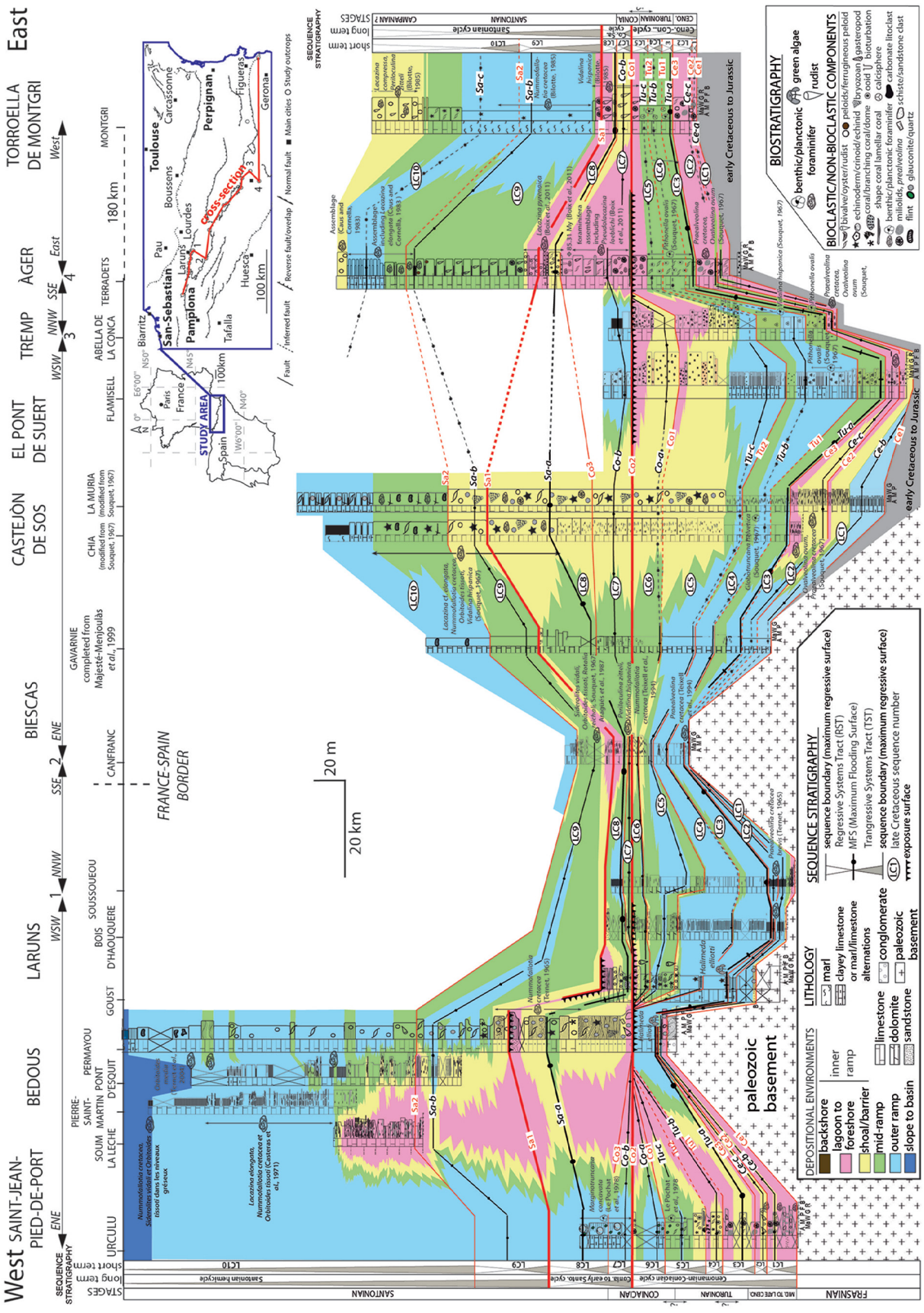

Fig. 8. Correlation diagram of Cenomanian to Santonian sections along the transect of this study. This diagram incorporates 14 outcrop sections examined in this study and 2 sections modified from Souquet (1967) (Chià and la Muria; locations in Fig. 1). Correlations are based on biostratigraphy (Fig. 3) and 10 recognized stratigraphic cycles (LC1 to LC10) delimited by maximum regressive surfaces (Ce1 to Sa2).

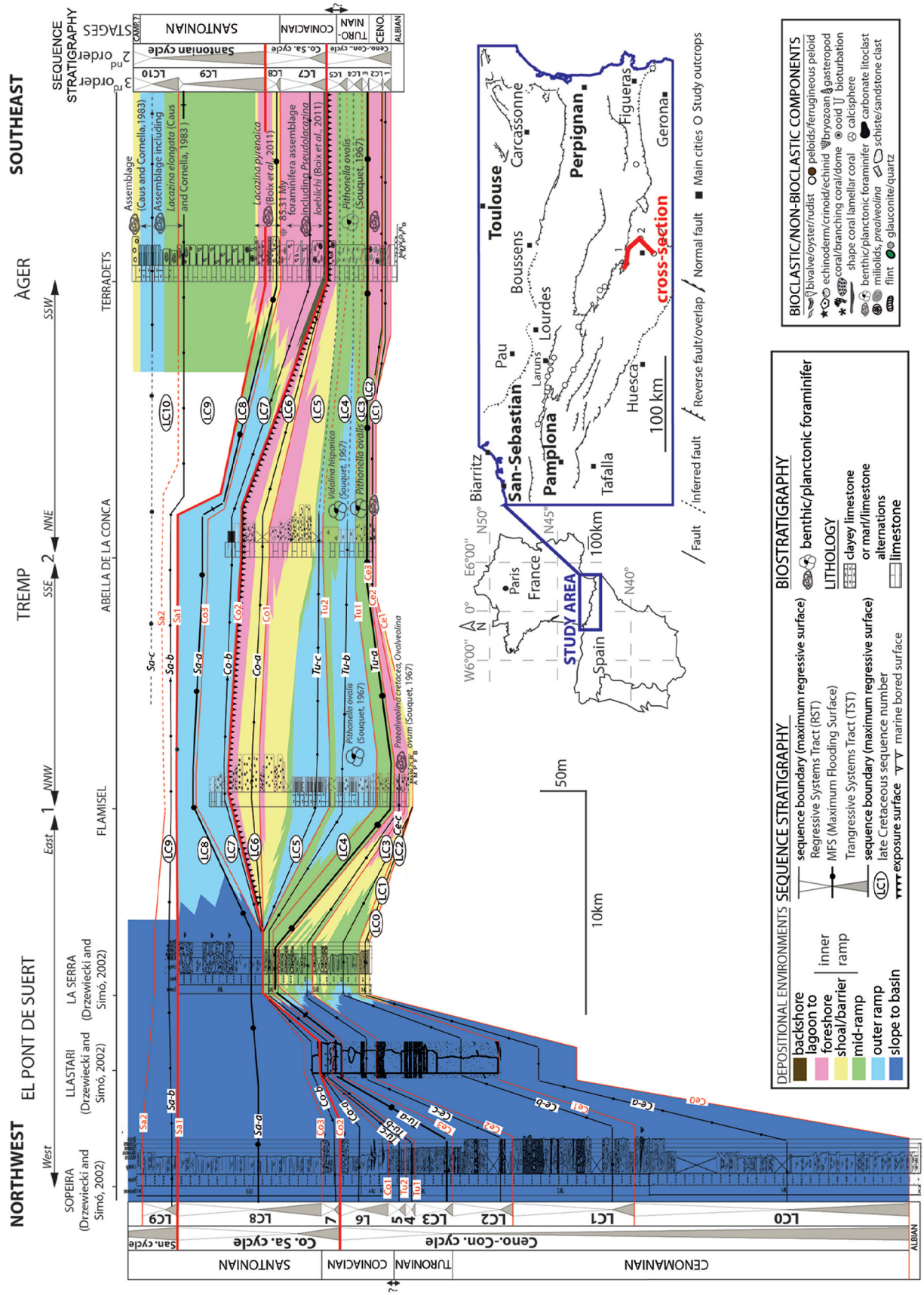

Fig. 9. Correlation diagram of Cenomanian to Santonian sections from the Iberian shallow margin to the basin, on a north-south transect from Àger to El Pont de Suert. This diagram incorporates three outcrop sections examined in this study and three sections from Drzewiecki and Simó (2002) (La Serra, Llastari and Sopeira; locations in Fig. 1). Correlations are based on biostratigraphy (benthic and planktonic foraminifera) and 11 recognized stratigraphic cycles (LC0 to LC10) delimited by maximum regressive surfaces (Ce0 to Sa2).

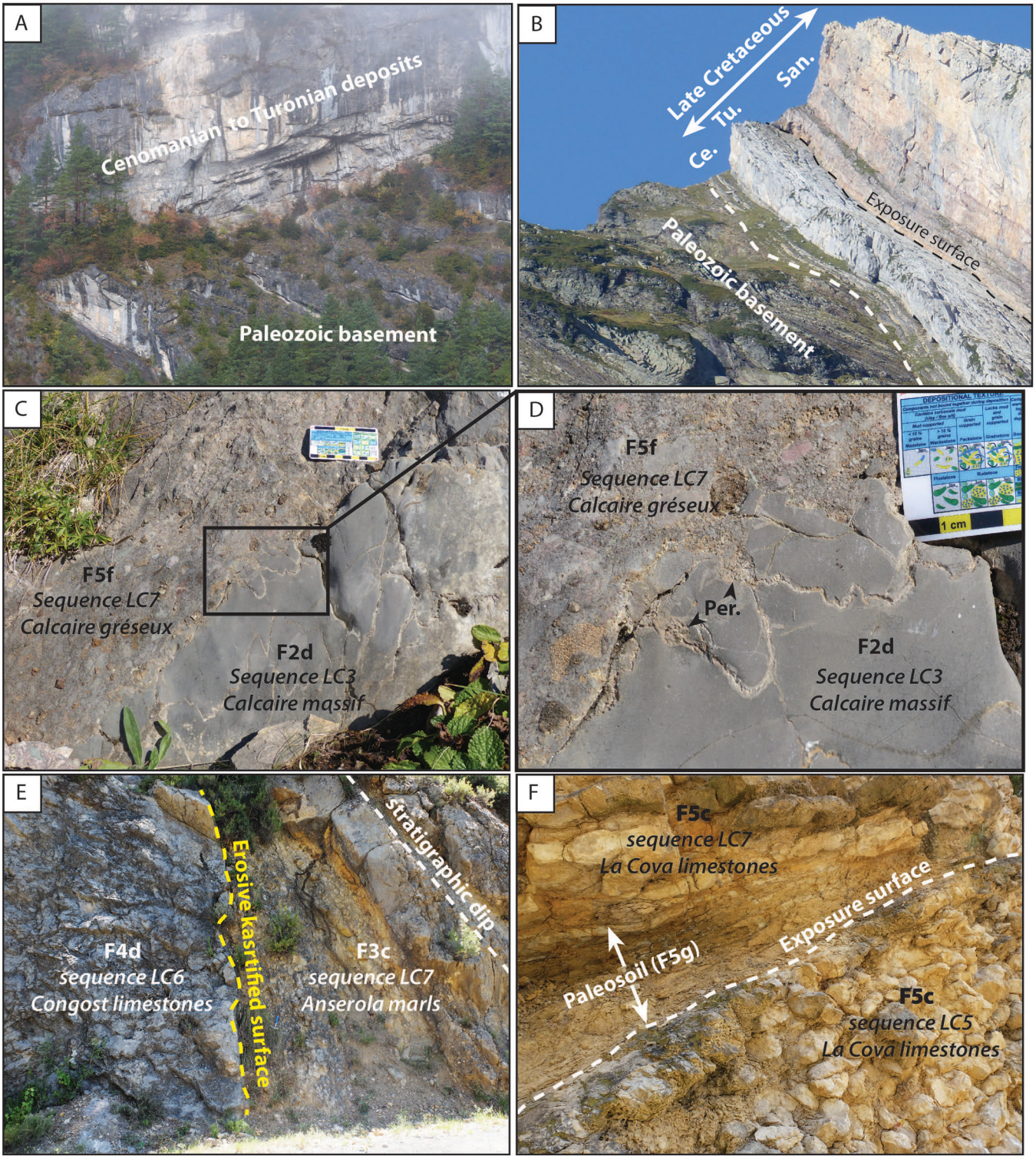

Fig. 10. A. Unconformity of Cenomanian to Turonian deposits on Paleozoic basement, Canfranc section, Calcaire lité member of the Calcaires des cañons Formation, sequences LC1 to LC4. B. Erosive unconformity of Upper Cretaceous deposits on Paleozoic basement, Permayou section, Calcaires des cañons Formation, sequences LC1 to LC9. C and D. Erosive sedimentary discontinuity between Calcaire massif member (facies F2d) and Calcaire gréseux member (facies F5f) of the Calcaires des cañons Formation, Permayou section, sequences LC1 and LC7. Sedimentary hardground displays perforations (Per.). E. Erosive karstified surface at the top of the Congost Formation (facies F4d) overlain by bivalve wackestone (facies F3c) of the Anserola Formation, Flamisell section, sequences LC6 and LC7. F. Exposure surface covered by a paleosol horizon (facies F4g), Terradets section, La Cova Formation, sequences LC5 and LC7.

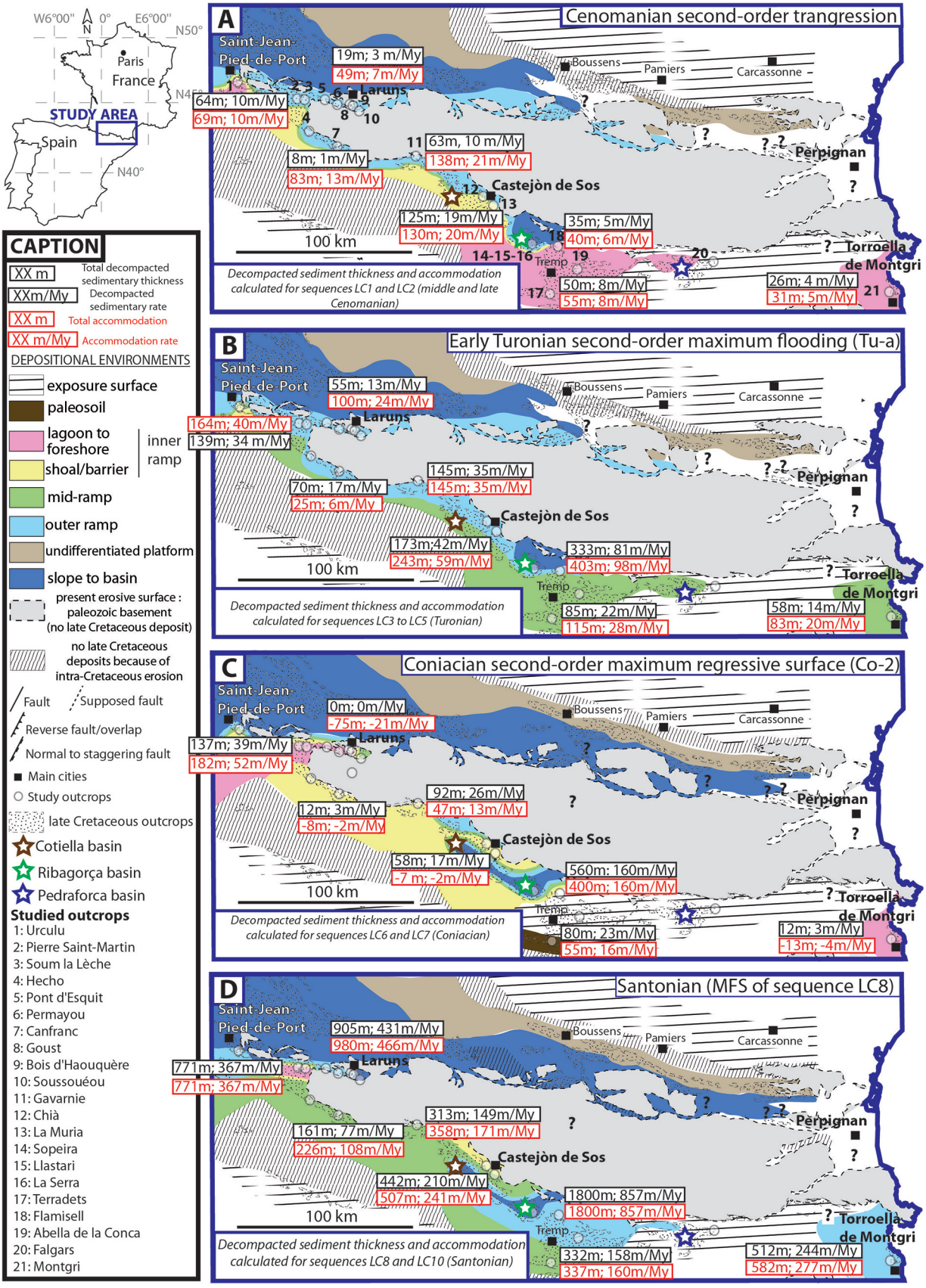
W6°00"
0°
E6°00"
N50°
N4
N40°
Paris
France
STUDY AREA
Spain
A
Cenomanian second-order trangression
Saint-Jean-Pied-de-Port
19m; 3 m/My
49m; 7m/My
64m; 10m/My
69m; 10m/My
Laruns
Boussens
Pamiers
Carcassonne
Perpignan
8m; 1m/My
83m; 13m/My
63m, 10 m/My
138m; 21m/My
Castejòn de Sos
125m; 19m/My
130m; 20m/My
35m; 5m/My
40m; 6m/My
100 km
14-15-16
Tremp
Torroella de Montgri
Decompacted sediment thickness and accommodation calculated for sequences LC1 and LC2 (middle and late Cenomanian)
50m; 8m/My
55m; 8m/My
26m; 4 m/My
31m; 5m/My
B
Early Turonian second-order maximum flooding (Tu-a)
55m; 13m/My
100m; 24m/My
164m; 40m/My
139m; 34 m/My
145m; 35m/My
145m; 35m/My
70m; 17m/My
25m; 6m/My
173m;42m/My
243m; 59m/My
333m; 81m/My
403m; 98m/My
Decompacted sediment thickness and accommodation calculated for sequences LC3 to LC5 (Turonian)
85m; 22m/My
115m; 28m/My
58m; 14m/My
83m; 20m/My
C
Coniacian second-order maximum regressive surface (Co-2)
0m; 0m/My
-75m; -21m/My
137m; 39m/My
182m; 52m/My
92m; 26m/My
47m; 13m/My
12m; 3m/My
-8m; -2m/My
58m; 17m/My
-7 m; -2m/My
560m; 160m/My
400m; 160m/My
Decompacted sediment thickness and accommodation calculated for sequences LC6 and LC7 (Coniacian)
80m; 23m/My
55m; 16m/My
12m; 3m/My
-13m; -4m/My
D
Santonian (MFS of sequence LC8)
905m; 431m/My
980m; 466m/My
771m; 367m/My
771m; 367m/My
313m; 149m/My
358m; 171m/My
161m; 77m/My
226m; 108m/My
442m; 210m/My
507m; 241m/My
1800m; 857m/My
1800m; 857m/My
Decompacted sediment thickness and accommodation calculated for sequences LC8 and LC10 (Santonian)
332m; 158m/My
337m; 160m/My
512m; 244m/My
582m; 277m/My
CAPTION
XX m
Total decompacted sedimentary thickness
XXm/My
Decompacted sedimentary rate
XX m
Total accommodation
XX m/My
Accommodation rate
DEPOSITIONAL ENVIRONMENTS
exposure surface
paleosoil
lagoon to foreshore
shoal/barrier
inner ramp
mid-ramp
outer ramp
undifferentiated platform
slope to basin
present erosive surface : paleozoic basement (no late Cretaceous deposit)
no late Cretaceous deposits because of intra-Cretaceous erosion
Fault
Supposed fault
Reverse fault/overlap
Normal to staggering fault
Main cities
Study outcrops
late Cretaceous outcrops
Cotiella basin
Ribagorça basin
Pedraforca basin
Studied outcrops
1: Urculu
2: Pierre Saint-Martin
3: Soum la Lèche
4: Hecho
5: Pont d'Esquit
6: Permayou
7: Canfranc
8: Goust
9: Bois d'Haouquère
10: Soussouéou
11: Gavarnie
12: Chià
13: La Muria
14: Sopeira
15: Llastari
16: La Serra
17: Terradets
18: Flamisell
19: Abella de la Conca
20: Falgars
21: Montgri

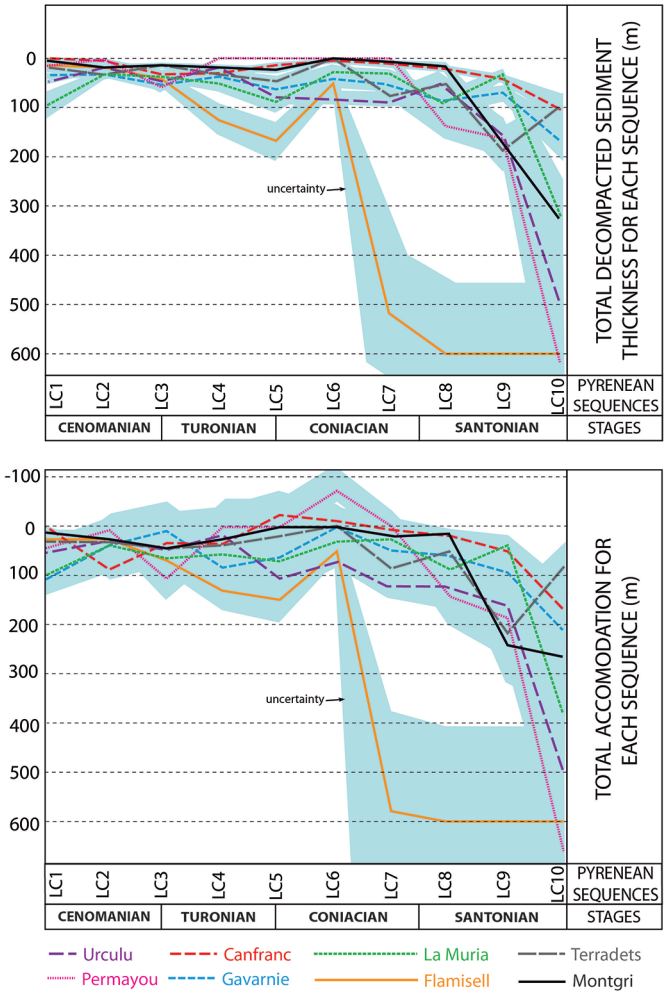

Fig. 12. Total decompacted sediment thickness and total accommodation for the eight sections in Figure 11 in the Cenomanian to Santonian interval.

Pyrenean rift system and European margin (Tugend *et al.*, 2014, 2015; Angrand *et al.*, 2018) and five previously published restored cross-sections along the strike of the orogen (Fig. 13; Mouthereau *et al.*, 2014; Teixell *et al.*, 2016; Grool *et al.*, 2018; Espurt *et al.*, 2019; Ternois *et al.*, 2019). By pinning these restored cross-sections to the European plate, we were able to use their restored geometry to reconstruct the width and shapes of Pyrenean rift system. Our reconstruction assumes that no major horizontal movement occurred between the end of rifting (Cenomanian) and the onset of the Pyrenean orogeny.

In our reconstructed map (Fig. 13), the Europe and Iberia plates were separated at that time by an area of exhumed sublithospheric mantle ~50 km wide (*e.g.*, Lagabrielle *et al.*, 2010; Clerc *et al.*, 2012), a width recently supported by numerical modeling (Jourdon *et al.*, 2019; Gómez-Romeu *et al.*, 2019). The Toulouse and Pamplona faults are inherited Variscan to Permian crustal-scale lineaments (Burg *et al.*, 1994; Saspiturry *et al.*, 2019b) that appear to separate crustal domains with distinct sedimentation histories (Razin, 1989). The Pyrenean rift was asymmetric (*e.g.*, Mouthereau *et al.*, 2014; Teixell *et al.*, 2018), such that the European necking domain was wider than the Iberian necking domain (~30–50 km vs ~10–20 km). The belt of exhumed mantle coincides with the deep turbiditic basin of Vacherat *et al.* (2017). On the Iberian margin, the future Axial Zone corresponds to an epicontinental marine facies (Barnolas *et al.*, 2015).

To locate our study outcrops on the restored map, we divided them into two groups according to their structural position. Outcrops with stratigraphic sections resting upon Paleozoic basement of the Axial Zone (Urculu, Pierre Saint-Martin, Soum la Lèche, Hecho, Pont d'Esquit, Permayou, Canfranc, Goust, Bois d'Haouquère, Soussouéou, Gavarnie, Chià and La Muria) were restored onto the Axial Zone. The other outcrops (Sopeira, Llastari, La Serra, Terradets, Flamisell, Abella de la Conca, Falgars and Montgri) were considered part of the South Pyrenean Zone sedimentary cover, detached by sliding within underlying Upper Triassic evaporites (*e.g.*, López-Mir *et al.*, 2014; Cámara and Flinch, 2017). These latter outcrops were shifted southward by about 10 km to take into account the displacement between the Axial Zone and the South Pyrenean Zone sedimentary cover (Grool *et al.*, 2018; Espurt *et al.*, 2019). It is noteworthy that although these outcrops are now located in the southern Pyrenees (Fig. 1), they have been restored to a position above the crustal units of the Axial Zone.

For the sake of this study, we correlate the facies environments with the main structural units of the rift system. Thus the deep oceanic basin corresponds to the deepest part of the basin and the necking and exhumed mantle domains. The platform-to-basin transition roughly corresponds to the necking zone. Closer to the craton, the shallow-marine epicontinental facies corresponds to the proximal domain.

4.4.2 Evolution of sedimentation and accommodation in the Pyrenean domain

We combined published records of sedimentation in the Pyrenean domain with the results of our outcrop studies to map the regional evolution of accommodation rates in the Cenomanian, Turonian, Coniacian and Santonian stages. Accommodation values for each stage are calculated from the 8 sites of Section 4.3 and 20 published sedimentary sections that are listed in Table 2. From this set of data, we identified seven palinspastic domains with distinct accommodation rates and sedimentary evolution: the southern Iberian platform, the northern Iberian platform, the western Iberian platform, the platform/basin transition, the basin, the eastern Aquitaine platform and the western Aquitaine platform. In addition to the sedimentary sections of the northern and southern Iberian platform domains in Figures 8 and 9, key

Fig. 11. Distribution of paleoenvironments in the Pyrenees in four successive steps from Cenomanian to Santonian: (A) Cenomanian second-order transgression, (B) early Turonian second-order maximum flooding, (C) Coniacian second-order maximum regressive surface and (D) Santonian maximum flooding surface of sequence LC8. Facies distribution is from this study and data from Barnolas *et al.* (2015). Sedimention and accommodation rates are calculated for each stage (A: Cenomanian; B: Turonian; C: Coniacian and D: Santonian) for eight characteristic sections from west to east: Urculu, Permayou, Canfranc, Gavarnie, La Muria, Flamisell, Terradets and Montgri.

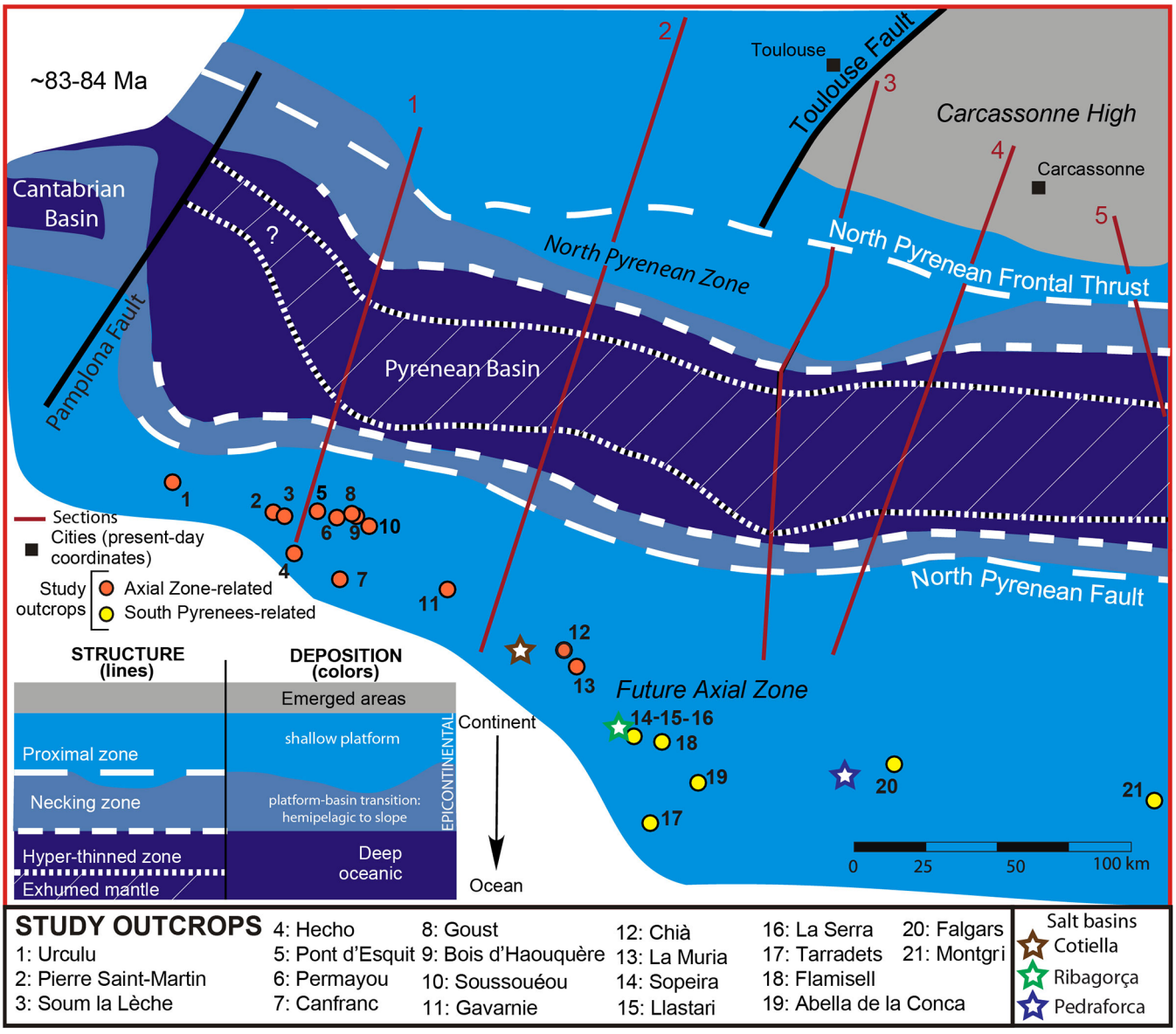

Fig. 13. Paleogeographic reconstruction of the Pyrenean rift margins at the pre-orogenic stage (~83–84 Ma). Structural areas are from Tugend *et al.* (2014) and Angrand *et al.* (2018) for the European plate. The widths of the necking zones and exhumed mantle domain between Europe and Iberia are minimum values based on restored cross-sections 1 (Teixell *et al.*, 2016), 2 (Espurt *et al.*, 2019), 3 (Mouthereau *et al.*, 2014), 4 (Grool *et al.*, 2018) and 5 (Ternois *et al.*, 2019). Study outcrops have been relocated according to their assigned structural domain (Axial Zone or South Pyrenean Zone). Depositional zones are from Barnolas *et al.* (2015) and this study.

sections from the basin and the eastern and western Aquitaine platform domains are illustrated in Figure 14. The evolution of accommodation rates for each domain is represented in Figure 15, and Figure 16 integrates the stage-level evolution of accommodation on a map of the seven palinspastic domains.

The southern Iberian platform domain includes six sites from this study and one from the literature. It has low median accommodation rates in the Cenomanian (13 m/My) and Turonian (24 m/My). The Coniacian accommodation rate decreases significantly, varying from 16 m/My in the Terradets section to −21 m/My in the Permayou section for a median value of −2 m/My. Accommodation rate increases sharply in the Santonian to a median value of 193 m/My.

The northern Iberian platform domain includes one site from this study and three from the literature, located near the boundary between platform and basin environments. This domain has low median accommodation rates in the Cenomanian (20 m/My) and Turonian (40 m/My). The rate increases sharply to 131 m/My in the Coniacian and 612 m/My in the Santonian, with values varying from 214 m/My in Sopeira to 1430 m/My in the Cotiella basin (Figs. 15B–G and 16).

Table 2. Locations and details of sites used to reconstruct the Cenomanian–Santonian evolution of sedimentation around the France-Spain boundary.

Paleogeographic location	Modern location (city)	Age	Depositional environment	Lithology/carbonate producers	Reference
Platform/basin transition	Arbas	Cenomanian to Coniacian	Slope to basin	Turbidites, marl, slope breccia	Barnolas *et al.* (2015)
	Errozate	Cenomanian to Santonian	Slope	Slope breccia	Merle (1974)
	Irun	Cenomanian to Santonian	Slope to basin	Turbidites, slope breccia	Barnolas *et al.* (2015)
	Massat	Cenomanian to Coniacian	Slope to basin	Turbidites, marl, slope breccia	Barnolas *et al.* (2015)
Basin	Biscaye	Cenomanian to Santonian	Basin	Turbidites	Barnolas *et al.* (2015)
	Hendaye/Saint-Jean-de-Luz	Cenomanian to Santonian	Basin	Turbidites	Razin (1989), Barnolas *et al.* (2015)
	Lourdes	Cenomanian to Santonian	Basin	Turbidites	Casteras *et al.* (1970)
	Mauléon	Cenomanian to Santonian	Basin	Turbidites	Le Pochat *et al.* (1976)
Western Aquitaine platform	Landes de Siougos	Cenomanian to Santonian	Shallow platform	Limestone, dolomite, marl	Serrano (2001)
	Mirande	Cenomanian to Santonian	Platform	Sandstone and limestone	Dubois and Seguin (1978)
	Roquefort	Cenomanian to Santonian	Platform	Limestone, dolomite, marl	Platel (1990)
	Canfranc	Cenomanian to Santonian	Platform	Limestone, sandstone	This study
	Falgars	Santonian	Platform	Limestone, sandstone	This study
	Gavarnie	Cenomanian to Santonian	Platform	Limestone, dolomite, marl	This study
Southern Iberian platform	La Muria	Cenomanian to Santonian	Platform	Marl, limestone (bioclastic wackestone to grainstone)	This study
	La Serra	Cenomanian to Santonian	Platform to basin	Marl, limestone (bioclastic wackestone to grainstone)	Drzewiecki and Simó (2002)
	Montgri	Cenomanian to Santonian	Shallow platform	Coral, planktonic foraminifera limestone, rudist limestone, marl	This study
	Permayou	Cenomanian to Santonian	Shallow platform	Bioclastic limestone, siliciclastic limestone, sandstone, clayey limestone	This study
	Terradets	Cenomanian to Santonian	Shallow platform	Marl, planktonic foraminifera limestone, rudist limestone, paleosol	This study
Eastern Aquitaine platform	Fontfroide (Corbières)	Cenomanian to Santonian	Shallow marine to continental	Lignite, reef limestone, sandstone	Bilotte (1985)
	Rennes-les-Bains (Corbières)	Cenomanian to Santonian	Marine platform: offshore to shallow marine	Marl-limestone alternations, limestone, sandstone, conglomerate	Bilotte (1985)
	Saurat	Cenomanian to Coniacian	Platform (Cenomanian and Turonian) to basin (Coniacian)	Turbidites, marl, reef limestone	Barnolas *et al.* (2015)
Northern Iberian platform	Cotiella	Cenomanian to Coniacian	Platform (Cenomanian to early Coniacian) and basin (late Coniacian to Santonian)	Limestone, marl, and slope breccia	López-Mir *et al.* (2014)
	Flamisell	Cenomanian to Santonian	Platform to basin	Marl, reef limestone, rudist limestone, planktonic foraminiferal limestone	This study
	Sopeira	Cenomanian to Santonian	Slope to basin	Marl, slope breccia	Drzewiecki and Simó (2002)
	Urculu	Cenomanian to Santonian	Platform (Cenomanian and Turonian) to basin (Coniacian and Santonian)	Flysch, marl, reef limestone, sandstone	This study
Western Iberian platform	Pancorbo	Cenomanian to Santonian	Shallow platform	Coral, rudist and dolomitic limestone	Barnolas *et al.* (2015)
	Sobròn	Cenomanian to Santonian	Shallow platform	Coral, rudist and dolomitic limestone	Barnolas *et al.* (2015)
	Zadorra	Cenomanian to Santonian	Outer platform	Marl and clayey limestone	Barnolas *et al.* (2015)

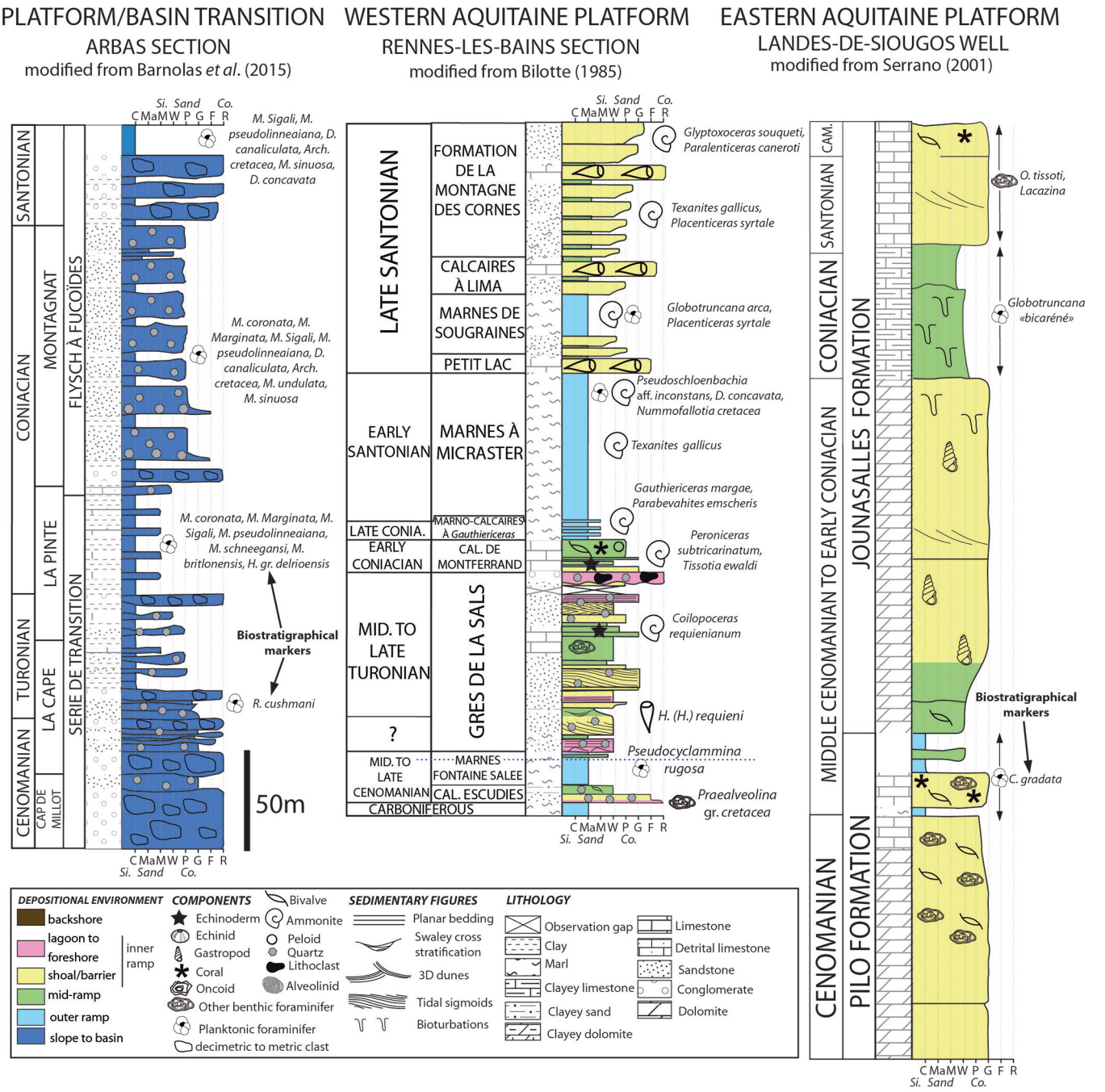

Fig. 14. Key sedimentary sections from the platform-basin transition (Arbas section, modified from Barnolas *et al.*, 2015), western Aquitaine platform (Rennes-les-Bains section, modified from Bilotte, 1985) and eastern Aquitaine platform (Landes-de-Siougos well, modified from Serrano, 2001).

The western Iberian platform domain includes three sites from the literature. It has moderate accommodation rates without major temporal variations; median values range from 32 m/My in the Coniacian to 73 m/My in the Turonian.

The eastern Aquitaine platform domain includes three sites from the literature. It has low median accommodation rates in the Cenomanian (11 m/My) and Turonian (16 m/My), then increases in the Coniacian (75 m/My) and Santonian (313 m/My). The greatest accommodation rates in this domain (457 m/My) are in the Fontfroide section in the Santonian.

The western Aquitaine platform domain includes three sites from the literature. It has relatively constant and low accommodation rates, with median values varying from 15 m/My to 38 m/My.

The platform/basin transition domain includes four sites from the literature, consisting of breccias alternating with marl beds and turbidites. It has low decompacted sedimentation rates between 28 m/My and 36 m/My from the Cenomanian to the Coniacian. The decompacted sedimentation rate doubles in the Santonian, approaching 70 m/My.

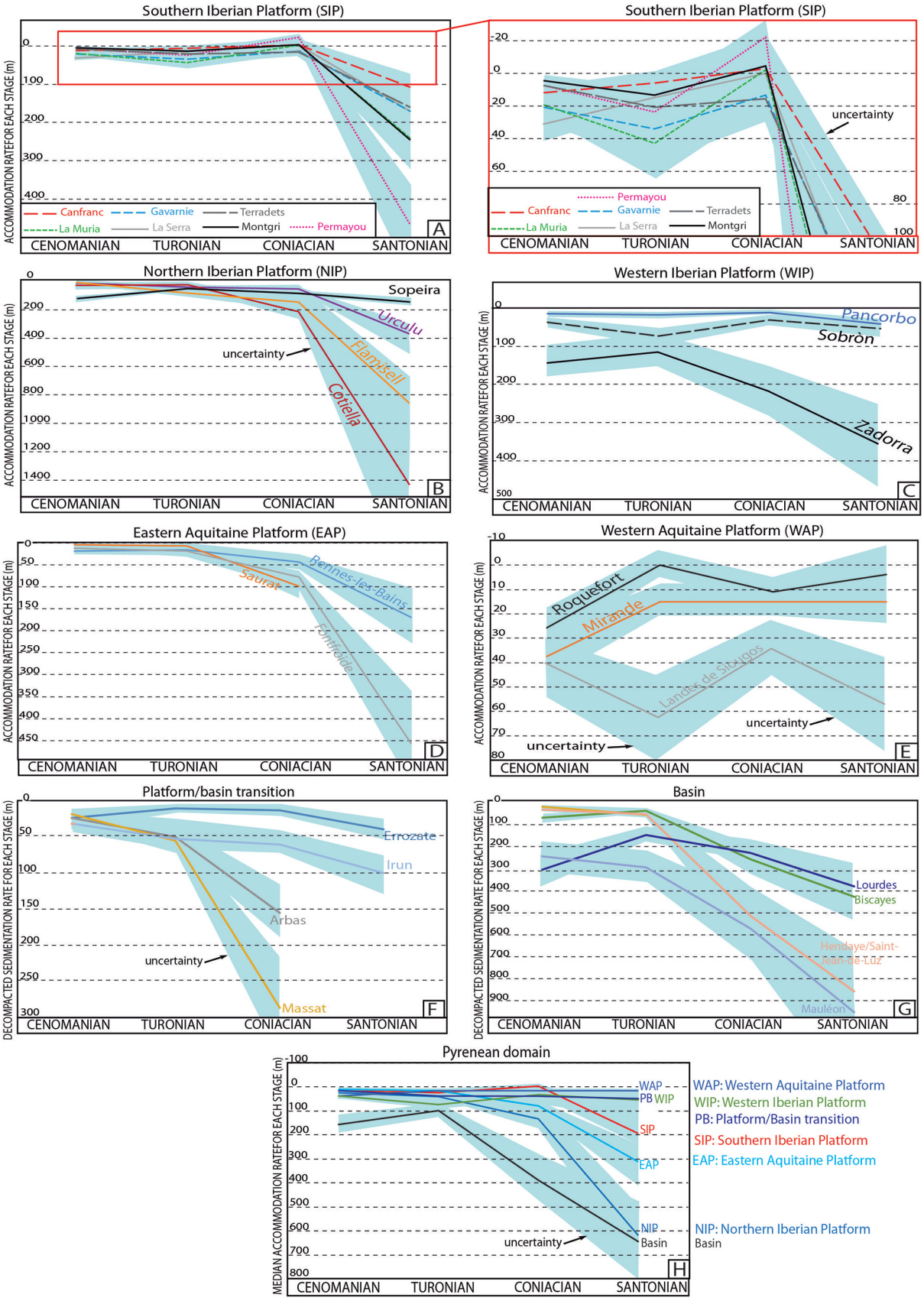
Southern Iberian Platform (SIP)
ACCOMMODATION RATEFOR EACH STAGE (m)
Canfranc
Gavarnie
Terradets
La Muria
La Serra
Montgri
Permayou
CENOMANIAN
TURONIAN
CONIACIAN
SANTONIAN
A
uncertainty
Northern Iberian Platform (NIP)
Sopeira
Urculu
Flamisell
Cotiella
B
Western Iberian Platform (WIP)
Pancorbo
Sobron
Zadorra
C
Eastern Aquitaine Platform (EAP)
Saurat
Bennes-les-Bains
Pontfolide
D
Western Aquitaine Platform (WAP)
Roquefort
Mirande
Landes de Sinsigos
E
Platform/basin transition
DECOMPACTED SEDIMENTATION RATE FOR EACH STAGE (m)
Errozate
Irun
Arbas
Massat
F
Basin
Lourdes
Biscayes
Hendaye/Saint-Jean-de-Luz
Mauleon
G
Pyrenean domain
MEDIAN ACCOMMODATION RATEFOR EACH STAGE (m)
WAP
PB WIP
SIP
EAP
NIP
Basin
H
WAP: Western Aquitaine Platform
WIP: Western Iberian Platform
PB: Platform/Basin transition
SIP: Southern Iberian Platform
EAP: Eastern Aquitaine Platform
NIP: Northern Iberian Platform

The basin domain includes four sites from the literature, consisting of thick distal turbidites. Its median decompacted sedimentation rate is moderate in the Cenomanian (155 m/My) and Turonian (100 m/My), then increases in the Coniacian (386 m/My) and again in the Santonian (643 m/My). Accommodation rates are highest in the Mauléon Basin, varying from 242 m/My in the Cenomanian to 952 m/My in the Santonian. Because Upper Cretaceous sediments survive only at the northern and southern edges of the basin, major uncertainties remain about the decompacted sedimentation rates in the center of the basin.

5 Discussion

5.1 Accommodation changes: eustasy or tectonics?

Platform sedimentary architecture, facies and accommodation rates change through time in the Pyrenean domain from the Cenomanian to the Santonian. These parameters depend directly on the ratio between accommodation and sedimentation rate, the first generated by changes in global eustasy and/or subsidence and the second generated by detrital input or in-situ carbonate production and its redistribution (Jervey, 1988; Schlager, 1993, 2005; Catuneanu *et al.*, 2009). Figure 17 summarizes our estimates of these parameters, presented in Section 4, along with eustatic variations during the Late Cretaceous as modeled by Miller *et al.* (2005) and Haq (2014).

Because long-term accommodation variations are not correlated with the eustatic curves (Fig. 17), they must instead be explained by local variations of subsidence rates. For instance, the Santonian has a consistently low eustatic sea level, which should lead to low to negative accommodation (Miller *et al.*, 2005; Haq, 2014), yet the sedimentary record indicates a strong increase in accommodation rates (Fig. 17). Moreover, the high spatial variability of accommodation rates in the different domains identified here, with sometimes opposite trends in accommodation, can only be explained by regional variations of subsidence. The eustatic variations and their amplitudes differ according to the authors (Fig. 17; Miller *et al.*, 2005; Haq, 2014), which makes their use in subsidence calculations questionable. Nevertheless, the magnitude of second order eustatic variations, the temporal resolution that interests us here, are about 25 m, which is much lower than the order of magnitude of the accommodation variations recorded during the Coniacian and Santonian (sometimes several hundred of meters; Figs. 15–17). In the remainder of the manuscript, we will therefore consider the accommodation as reflecting, at first order, the evolution of subsidence in time and space.

Figures 15–17 outline the following history of the palinspastic domains of the Pyrenean realm. In the Cenomanian and Turonian, the Iberian and Aquitaine platforms have low accommodation rates (median values of 22 m/My and 16 m/My, respectively, for the Cenomanian and 15 m/My and 28 m/My for the Turonian) and the basin domain has decompacted sedimentation rates several times greater (median values of 155 m/My for the Cenomanian and 100 m/My for the Turonian). In the Coniacian, three areas evolve in divergent ways: (1) the southern Iberian platform displays evidence of uplift in continental facies and sedimentation gaps (median accommodation value −2 m/My); (2) the basin, northern Iberian platform and eastern Aquitaine platform display evidence of subsidence (decompacted sedimentation rate of 386 m/My in the basin); and (3) the western Aquitaine and western Iberian platforms remain in a state of slow and steady subsidence (median accommodation rates of 15 m/My and 32 m/My, respectively). During the Santonian, subsidence increases substantially over nearly the entire Pyrenean domain (median accommodation rates from 193 m/My in the southern Iberian platform to 643 m/My in the basin), except in the western Iberian and western Aquitaine platforms (median accommodation rates of 54 m/My and 15 m/My, respectively).

5.2 Tectonics and large-scale accommodation changes in the Pyrenean domain

The Pyrenean domain displays major regional discrepancies in accommodation over the Cenomanian–Santonian interval (Figs. 15–17). In Coniacian time, the western Pyrenean domain records a large-scale increase of subsidence rates except in the southern Iberian platform, where the accommodation rate is negative. The eastern Pyrenean domain remains stable from the Cenomanian to the Coniacian. Finally, the Santonian is a stage with a universal increase in accommodation rate. In this section we discuss the tectonic origins of these and other variations, especially in the Coniacian and Santonian, as the possible result of four potential controls: (1) salt tectonics, (2) postrift thermal subsidence, (3) renewed extension and (4) the onset of Europe-Africa convergence.

5.2.1 Salt tectonics and Iberian margin subsidence

Salt tectonics, which comprises diapirism, gravity-driven extensional faulting and cover gliding, implies first-order vertical movements that lead to (1) rapidly subsiding small basins (as fast as several kilometers per million years; *e.g.*, López-Mir *et al.*, 2014, 2015) and (2) local uplift over the head of rising diapirs (*e.g.*, Poprawski *et al.*, 2016). Throughout the Pyrenees, deposition of thick evaporitic series during the Late Triassic played a key role from the Jurassic to the Paleogene by controlling the position of tectonic detachments or décollements, causing diapirism or promoting gravity-driven extensional faulting (Brinkmann and Lögters, 1968; Hudec and Jackson, 2007; Saura *et al.*, 2016). From Cenomanian to Santonian time, salt tectonics is documented in the eastern Iberian platform in the Ribagorça Basin (Saura *et al.*, 2016; late Albian to late Santonian), the Cotiella Basin (López-Mir *et al.*, 2014, 2015; middle Coniacian to early Santonian) and the Pedraforca area (Vergés, 1993; Aptian and Cenomanian to Santonian) (locations in Figs. 1, 11 and 13). In the central part

Fig. 15. Accommodation or decompacted sedimentation rates for the Cenomanian to Santonian stages of sedimentary sections from (A) the southern Iberian platform (detail shown at right), (B) northern Iberian platform, (C) western Iberian platform, (D) eastern Aquitaine platform, (E) western Aquitaine platform, (F) platform-basin transition and (G) basin. Note differing vertical scales. H. Median accommodation rates for each domain.

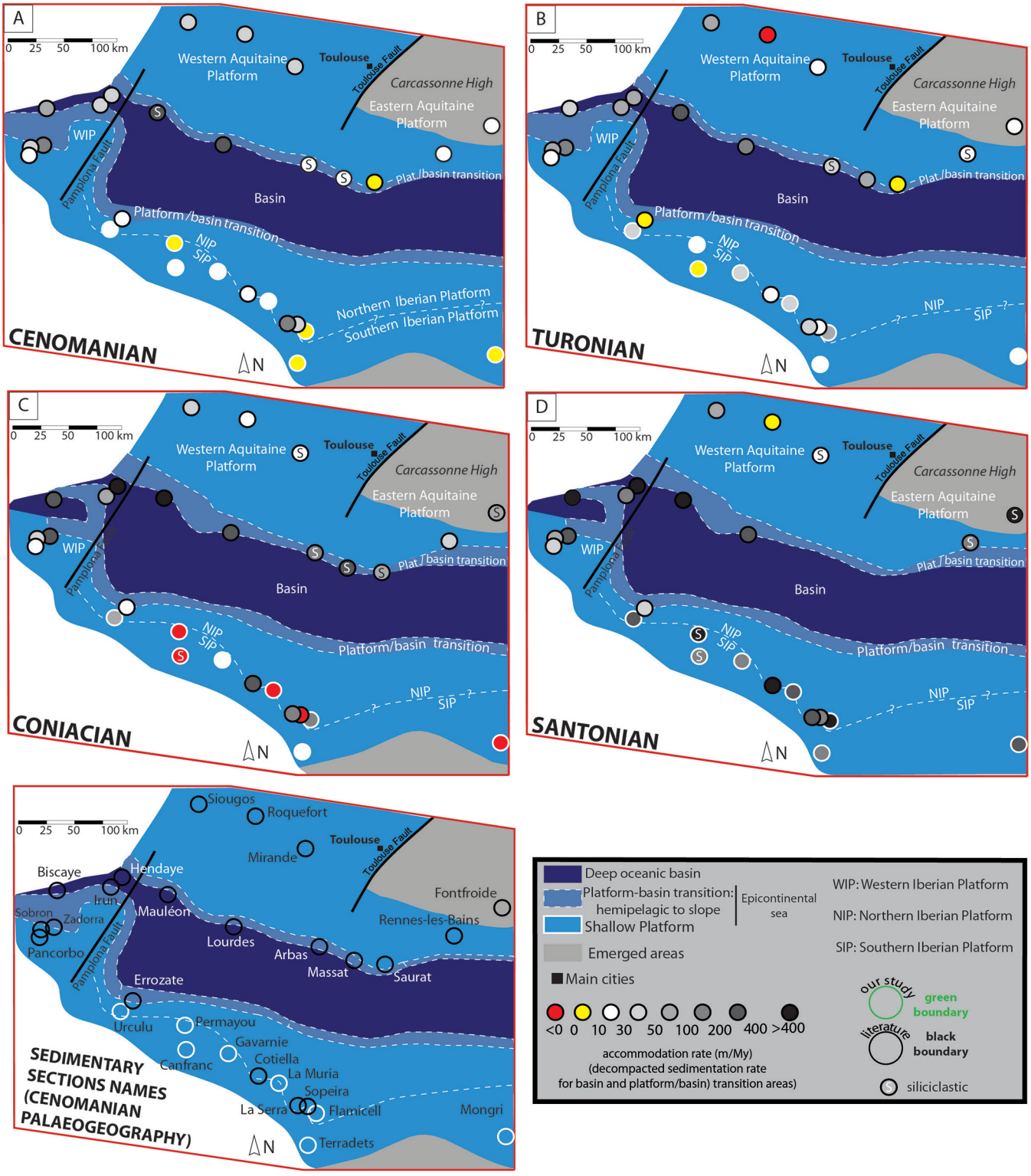

Fig. 16. Paleogeographic maps showing the evolution of accommodation rates in the Cenomanian, Turonian, Coniacian and Santonian along the Iberia-Eurasia plate boundary. Data sources are listed in Table 2.

of the Iberian platform, corresponding to the current Axial Zone, studied outcrops from Urculu to Gavarnie (localities 1 to 11) and Errozate (Merle, 1974) directly overlie Paleozoic rocks, and their accommodation rates were not influenced by vertical salt tectonics (Figs. 15 and 16). The outlying Montgri and Terradets sections, where Upper Cretaceous rocks overlie Albian limestone, likewise had no Triassic salt diapirs (Saura *et al.*, 2016). All of these sedimentary sections record a sharp decrease in accommodation rates in the Coniacian, including negative values, followed by an increase in the Santonian

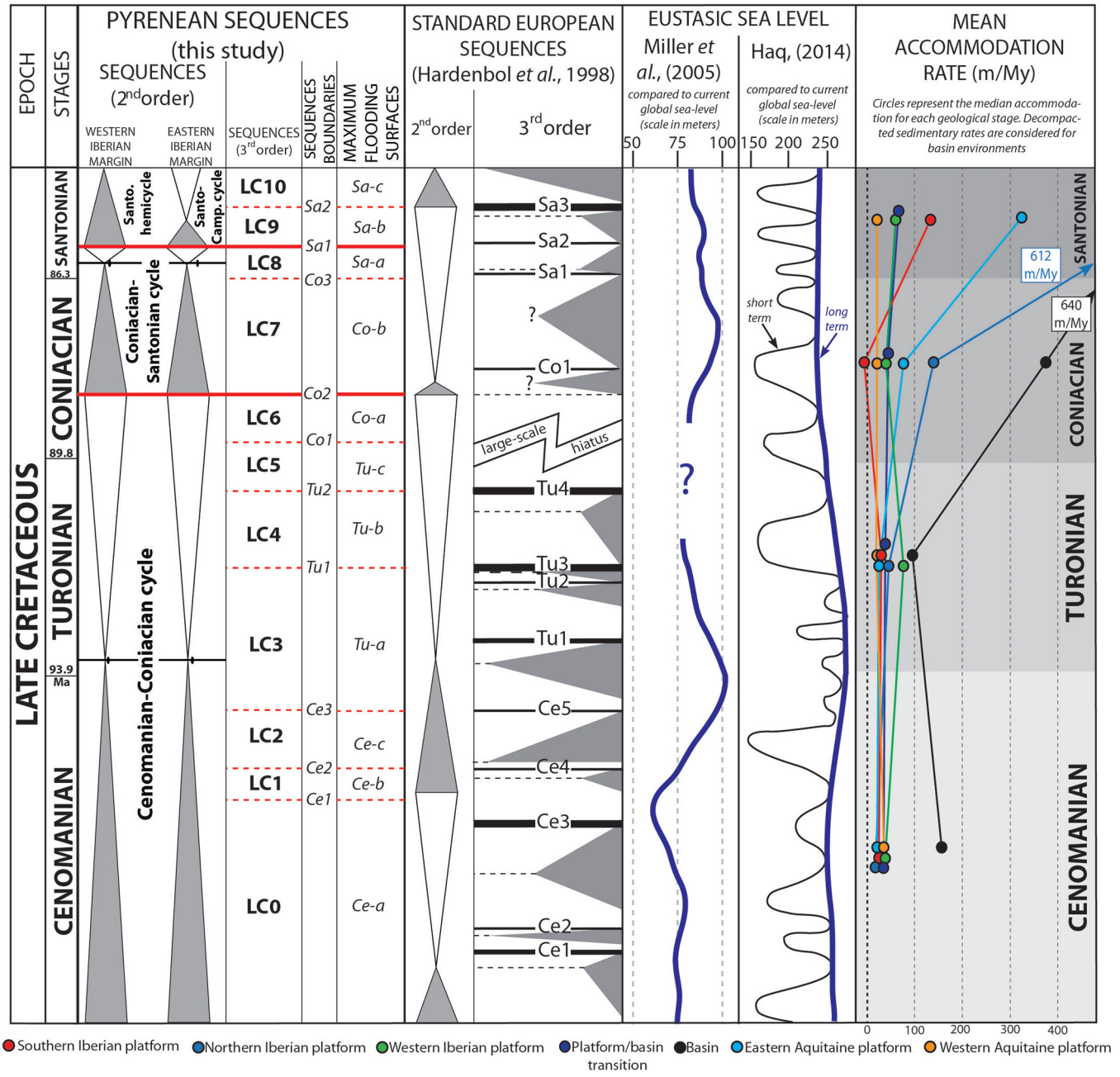

Fig. 17. Chronostratigraphic diagram from the Cenomanian to Santonian showing Iberian margin sequences, second- and third-order European sequences (Hardenbol *et al.*, 1998), eustatic sea-level curves (Miller *et al.*, 2005; Haq, 2014) and accommodation rates for the seven domains defined in this study.

(Figs. 15 and 16). The Urculu section, on the northern Iberian platform where Cenomanian limestones rest upon Paleozoic basement, likewise displays increased subsidence rates after the Coniacian. This finding shows that although salt tectonics did not control the large-scale vertical movements on the Iberian margin during the Coniacian and Santonian, it may have locally modified accommodation rates.

The deep and abrupt subsidence recorded in the Cotiella area in the late Coniacian and early Santonian is indisputably related to salt tectonics (López-Mir *et al.*, 2014, 2015). However, the La Muria section, near the Cotiella basin, displays a shallowing of depositional environments in the Coniacian associated with near-zero accommodation rates, followed by an increase in accommodation rates to about 240 m/My in the Santonian, comparable to sections unaffected by salt tectonics (Fig. 15A), indicating that the La Muria area was little affected by salt tectonics.

The Sopeira, La Serra and Flamisell sections are located in the Ribagorça basin, which contains the minibasins of Sopeira and Sant Gervàs. The Sopeira minibasin formed consequently to the rise of the Aulet diapir during Albian and Cenomanian time, leading to a high subsidence rate (130 m/My at La Serra)

in the Cenomanian (Figs. 9, 15B and 16; Saura *et al.*, 2016). Coniacian subsidence rates are lower in the Sopeira minibasin as well as diapirism, as attested by the accommodation rates at Sopeira and La Serra (Figs. 9 and Figs. 9 and 15A, B). At this same time, a sharp increase in subsidence rates is recorded in the Sant Gervàs minibasin in response to the activation of the northward deepening Sant Gervàs salt detachment (Saura *et al.*, 2016). The Flamisell section, located a few kilometers west of Sant Gervàs peak, records an increase of accommodation rate to about 200 m/My in the Coniacian that explodes in the Santonian to more than 1100 m/My. This dramatic change is in all likelihood the consequence of salt tectonics in the nearby Sant Gervàs minibasin.

Salt tectonics implies locally very high subsidence rates, as in the Cotiella, Sopeira and Flamisell sedimentary sections, which are placed here in the northern Iberian platform domain. The Coniacian is marked by the development of north-dipping detachments rooted at depth in Upper Triassic to Hettangian evaporites in both the Cotiella and Ribagorça basins, interpreted as extensional basins (López-Mir *et al.*, 2014, 2015; Saura *et al.*, 2016). Large-scale uplift of the southern Iberian margin and increased subsidence rates in the oceanic basin occurred in the meantime (Figs. 15 and 16). The geometric result was a northward tilting of the Iberian margin that would have favored or initiated detachment faulting along salt décollements in the Cotiella and Ribagorça basins.

5.2.2 Post-rift thermal subsidence

Flexural subsidence in response to the load of the Pyrenean orogen is not sufficient to explain the subsidence recorded in the Aquitaine retro-foreland basin over the entire orogenic stage from the Campanian to the Miocene (Desegaulx and Brunet, 1990; Angrand *et al.*, 2018), nor does it explain the subsidence in the Ebro pro-foreland basin (Gaspar-Escribano *et al.*, 2001; Curry *et al.*, 2019). In the Aquitaine basin, north of the North Pyrenean Frontal Thrust (Fig. 1), postrift thermal subsidence has been proposed to contribute to the thickness of the foreland basin, especially in its central and western parts (Angrand *et al.*, 2018; Curry *et al.*, 2019). This thermal subsidence, inherited from the Early Cretaceous Pyrenean rifting, would have started in the late Cenomanian or early Turonian, at the end of rifting, and thus would have continued during the synorogenic phase (Angrand *et al.*, 2018). While this postrift thermal subsidence has been invoked to account for part of the subsidence in the Aquitaine basin, it probably does not explain the vertical motions in the Pyrenean domain recorded here.

Postrift thermal subsidence decreases with time as the lithosphere cools after rifting (*e.g.*, McKenzie, 1978; Royden and Keen, 1980; Bond *et al.*, 1983). If it was the main driver of subsidence in the Pyrenean domain, subsidence rates would have been high at the end of rifting in the Turonian and would have decreased during the Coniacian and Santonian ages. This study, instead, documented low subsidence rates in the Turonian, followed in the Coniacian by increased subsidence rates on the former margins of the Pyrenean rift, then a further increase in the Santonian, at which time the area of subsidence expanded to the Iberian and Aquitaine platforms. In addition, the Iberian margin was probably less thinned than the European margin (*e.g.*, Cochelin *et al.*, 2017) and therefore would have been less affected by postrift thermal subsidence. Finally, postrift cooling cannot explain the uplift that is recorded in the Iberian margin in the Coniacian (Figs. 15–17).

5.2.3 Renewed extension and Europe-Africa convergence

The commonly proposed geodynamic scenario suggests that convergence between Africa and Europe was partially accommodated through eo-alpine orogenesis (131–84 Ma) until the end of the Santonian, when convergence began in the Pyrenean domain (~84 Ma; Vergés *et al.*, 1992; Olivet, 1996; Srivastava *et al.*, 2000; Rosenbaum *et al.*, 2002; Sibuet *et al.*, 2004; Jammes *et al.*, 2009; Handy *et al.*, 2010; Vissers and Meijer, 2012; Mouthereau *et al.*, 2014; Macchiavelli *et al.*, 2017). This implies that the Pyrenean domain was tectonically quiescent from the end of rifting in the Albian and Cenomanian to the onset of compression in the late Santonian or later. However, the plate kinematic evolution of Iberia during the Cretaceous is controversial because very few high-quality paleomagnetic data are available to constrain kinematic reconstructions of Iberia during the Late Cretaceous, especially the Coniacian and Santonian (Neres *et al.*, 2012, 2013; Barnett-Moore *et al.*, 2016; Macchiavelli *et al.*, 2017).

This paper documents major spatial variations in subsidence rates in the Coniacian: the Iberian platform tilts northward as uplift of the southern Iberian platform coincides with increased subsidence rates in the northern Iberian platform, the basin and the eastern Aquitaine platform (Figs. 15 and 16). Here we evaluate two geodynamic cases that can explain this behavior: (1) extension leading to increased subsidence within the basin and uplift on its southern margin (southern Iberian platform) or (2) large-scale pre-orogenic north-south oriented compressive strain.

A Coniacian extension phase is inconsistent with Pyrenean geodynamic history and unsupported by field evidence. The Pyrenean rifting stage ends in the middle Cenomanian (Jammes *et al.*, 2009; Lagabrielle *et al.*, 2010; Masini *et al.*, 2014; Teixell *et al.*, 2016; Saspiturry *et al.*, 2019a, Issautier *et al.*, 2020), and extension is unlikely to resume in the Coniacian, after a late Cenomanian to Turonian quiescent stage and preceding the late Santonian onset of compressive deformation. No indications of extensive Coniacian deformation, such as normal faults rooting at depth in the basement (extensional thick-skinned tectonics), are known in the Pyrenean domain. The formation of north-dipping detachments rooted in Triassic and Hettangian evaporites in the Cotiella and Ribagorça basins (López-Mir *et al.*, 2014, 2015; Saura *et al.*, 2016) can be explained by northward tilting of the Iberian platform, as shown by accommodation rates, rather than by synrift extensional deformation (Figs. 15 and 16). Finally, a Coniacian extension stage would entail uplift of both the Iberian and European margins, but uplift is apparent only in the southern Iberian platform.

We argue that the Coniacian flexure and ensuing Santonian large-scale subsidence originate from compressive strain. We propose an evolution in three stages for the Pyrenees from the Cenomanian to the Campanian, as shown in Figure 18: a postrift stage (Cenomanian to Turonian), a transitional phase (Coniacian to early Santonian) and early orogeny (late Santonian to early Campanian).

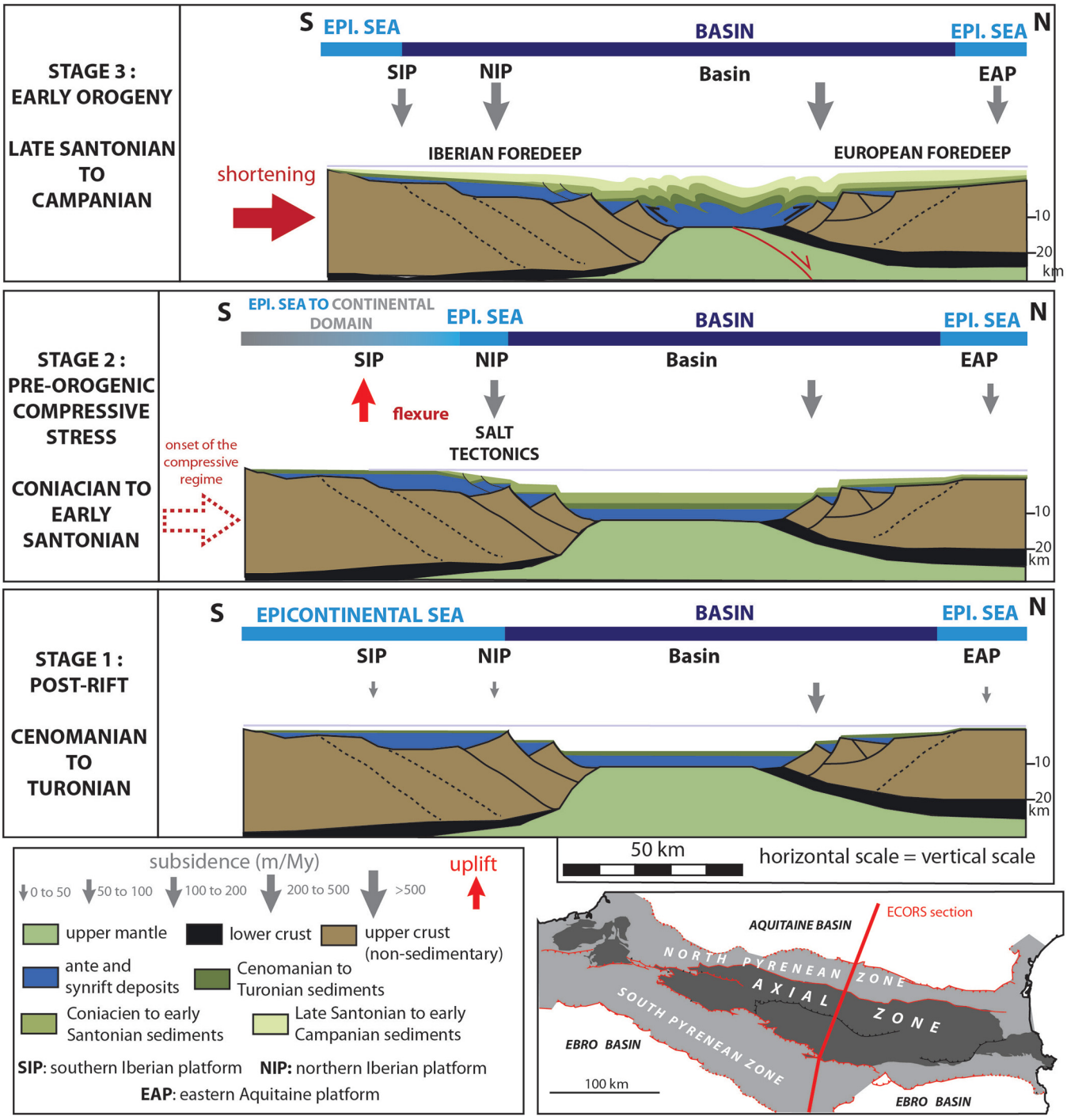

Fig. 18. Schematic south-north crustal profiles along the ECORS ("Étude Continentale et Océanique par Réflexion et Réfraction Sismique") section showing the geodynamic evolution of the eastern Pyrenees from the Cenomanian to the early Campanian (modified from Mouthereau *et al.*, 2014). No vertical exaggeration. Decompacted sedimentation rates and accommodation rates are calculated from sources listed in Table 2 for paleogeographic domains defined in this study.

The first stage is a classical postrift stage characterized by low subsidence rates on the Iberian and Aquitaine platforms and moderate subsidence rates in the Pyrenean turbiditic basin (Jammes *et al.*, 2009; Lagabrielle *et al.*, 2010; Masini *et al.*, 2014; Teixell *et al.*, 2016; Saspiturry *et al.*, 2019a).

The second stage features a reorganization of subsidence in the Pyrenean domain that can be the consequence of two geodynamic events: (1) the early initiation – during the Coniacian – of convergence between the Iberian and European plates and/or (2) a far-field stress related to ENE-directed Africa motion relative to Europe.

The progressive acceleration and generalization of subsidence in the Pyrenean realm from the Coniacian to Campanian could be explained by an initiation of the Iberia-Europe

convergence from the Coniacian, whereas it is until now considered as starting in the latest Santonian (Rosenbaum *et al.*, 2002; Sibuet *et al.*, 2004; Jammes *et al.*, 2009; Handy *et al.*, 2010; Vissers and Meijer, 2012; Mouthereau *et al.*, 2014; Macchiavelli *et al.*, 2017). Subsidence histories observed in other foreland basins (Xie and Heller, 2009; Escalona and Mann, 2011; Sinclair and Naylor, 2012) are similar to the history documented in this study: (1) a gradual passive margin subsidence (Cenomanian to Turonian) followed by (2) an abrupt increase in subsidence rates indicating the initiation of convergence (Coniacian) and (3) an increase of subsidence rates with time (Santonian). A similar scenario is documented by Bayona *et al.* (2013) in the eastern Cordillera of Colombia in response to Caribbean–South America plate convergence in the early Paleocene. There they identified an uplifting western domain (toward the plate boundary), a rapidly subsiding central domain and a slowly subsiding to uplifting eastern domain. Similar to the case in Colombia (Bayona *et al.*, 2013), the Aquitaine and Iberian platforms record an input of detrital material during the Coniacian (Fig. 16; Dubois and Seguin, 1978; Bilotte, 1985; Platel, 1987; Al Hamawi, 1992; Teixell *et al.*, 1994). However, there are limitations to the early initiation of Iberia-Europe convergence hypothesis since no field evidence of syn-sedimentary deformation is documented during the Coniacian or early Santonian (*e.g.* syntectonic folding), nor the beginning of the shortening of the basin domain. There are therefore no indications that this early compressive stage is synchronous with the convergence in the strict sense between the Iberian and European plates, *i.e.* a shortening of the exhumed mantle area. It is yet conceivable that deformation indices are no longer accessible today, for example if they are contained in the eastern part of the Pyrenean mountain belt, now dismantled (Gulf of Lion; Jolivet *et al.*, 2015, 2020) or in early basins that are poorly preserved today (*e.g.* central and eastern North Pyrenean Zone). Consequently, the hypothesis of a beginning of convergence between Iberia and Europe as early as the Coniacian, while not yet supported by arguments strong enough to be asserted, should not be excluded.

Although its details are poorly known owing to insufficient data between chrons M0 and C34 (*e.g.*, Rosenbaum *et al.*, 2002), ENE-directed motion of Africa is accommodated along a transcurrent corridor, inverting former Alpine Tethys domains. This transpressive regime evolves in a north-south compressive component between Apulia and Europe at this time (De Grasiansky *et al.*, 1989; Dewey *et al.*, 1989). The second hypothesis is that far-field stress related to ENE-directed Africa motion during the Coniacian to early Santonian led to the observed large-scale flexure characterized by northward tilting of the Iberian platform (uplift of the southern Iberian platform and rapid subsidence of the northern Iberian platform) and high subsidence rates in the basin and eastern Aquitaine platform domains (Fig. 18).

Tilting of the Iberian platform favors the development or reactivation of north-dipping décollements rooting in Triassic salt deposits and very high subsidence rates recorded in the Cotiella and Ribagorça basins during the Coniacian and early Santonian (Fig. 18; López-Mir *et al.*, 2014, 2015; Saura *et al.*, 2016). On a larger scale, the Coniacian is a time of major paleogeographical reorganization. In the Paris Basin, a large-scale flexure (wavelength ~300 km) occurred during the Coniacian in which the basin edges were uplifted while subsidence increased in the center of the basin (Lasseur, 2007). In the southern part of the Paris Basin, the flexure suggests SSW-NNE oriented strain that may represent a far-field effect of the initiation of Europe-Africa convergence (Lasseur, 2007).

In the third stage (late Santonian to early Campanian) of early orogenesis, compression and orogenic loading increases subsidence rates all over the Pyrenean domain, except at its western end (Figs. 17 and 18; Dubois and Seguin, 1978; Bilotte, 1985; Puigdefàbregas and Souquet, 1986; Puigdefàbregas *et al.*, 1992; Jammes *et al.*, 2009; Barnolas *et al.*, 2015). The shortening begins within the basin domain, and field evidence of Pyrenean deformation is documented on the eastern European platform (syntectonic folding in Provence; Leleu, 2005; Leleu *et al.*, 2009) and the Iberian platform (Mey *et al.*, 1968; Papon, 1969; Simó, 1986; Puigdefàbregas *et al.*, 1992). The eastern Aquitaine and north and south Iberian platforms form rapidly subsiding early foredeeps. In the western Aquitaine and western Iberian platforms, the limited data show lower subsidence rates that remain relatively constant from the Cenomanian to the Santonian. In the westernmost Pyrenees, the absence of shortening localized on thrusts, during the latest Santonian, suggests that Iberia-Eurasia plate convergence was regionally variable during this early orogenic stage. This contrast probably reflects the slightly earlier onset of convergence in the eastern and central Pyrenees where an early foreland basin formed, compared to the western part where postrift thermal subsidence persisted at that time (Figs. 15–17; Angrand *et al.*, 2018).

6 Conclusions

We documented changes in platform geometry, sedimentary facies and accommodation rates in Cenomanian to Santonian formations on the basis of field observations at 11 outcrop sequences in a 400-km transect of the Iberian margin of the Pyrenees. To these findings we added previously published sedimentation and accommodation rates in the Late Cretaceous Pyrenean domain, including the Pyrenean turbiditic basin, the Iberian platform and the Aquitaine platform. This information allows us to infer the spatial and temporal evolution of subsidence rates in the Pyrenean domain, which we interpret in terms of three stages:

- a Cenomanian to Turonian postrift thermal subsidence stage is characterized by low accommodation rates in the Iberian and Aquitaine platforms (about 15 m/My to 30 m/My) and moderate accommodation rates in the Pyrenean turbiditic basin (about 100 to 150 m/My);
- a Coniacian to early Santonian stage is characterized by the formation of a flexure defined by uplift of the southern Iberian platform (negative accommodation rates) and sharply increased subsidence of the northern Iberian platform, Pyrenean turbiditic basin and eastern Aquitaine platform. Rejecting causes in local salt tectonics, thermal subsidence or episodic extension, we propose the onset of a compressive regime as the origin of this flexural response at the Iberia-Europe plate boundary. However, whether this is related to onset of shortening at the Iberia-Europe boundary in the central and eastern Pyrenees, to the the far-

field response to ENE motion of Africa relative to Europe, or the combined action of these two factors, remains uncertain;
– a late Santonian to Campanian stage is characterized by early orogenesis, marked by widespread flexural deformation and shortening. Accommodation rates are very high over the Pyrenean domain outside its western part. The eastern Aquitaine and Iberian platforms form early foredeeps, and early orogenic loading in the eastern Pyrenean basin leads to high subsidence rates that decrease to the west such that the western Aquitaine platform and Cantabrian basins are relatively stable.

We evidence for the first time a pre-orogenic (*i.e.* pre-late Santonian) flexure geometry at the Iberia-Europe plate boundary induced by regional plate reorganisation between stable Africa and stable Europe during the Coniacian and the early Santonian.

Acknowledgments. This study was conducted within the framework of the integrated geological Orogen research project (funded by Total S. A., BRGM, and INSU). We thank the Orogen project managers Isabelle Thinon (BRGM-French Geological Survey), Sylvain Calassou (Total), Emmanuel Masini (Total) and Olivier Vidal (CNRS). We are grateful to Thin Section Lab for the high-quality thin sections. Thanks to Guillaume Badinier for assistance during our fieldwork. We thank R. Blakey for the free access to paleogeographic maps at http://cpgeosystems.com. The authors thank the anonymous reviewer, Peter Drzewiecki and the guest editor Olivier Lacombe for their constructive comments that clearly contributed to improve the quality of this paper.

References

Al Hamawi M. 1992. Sédimentologie, pétrographie sédimentaire et diagenèse des calcaires du Crétacé supérieur de la marge ibérique. PhD Thesis. France: Bordeaux 1 University.

Allen A, Allen JR. 2005. Basin analysis. Oxford: Blackwell Science Publications.

Angrand P, Ford M, Watts AB. 2018. Lateral variations in foreland flexure of a rifted continental margin: the Aquitaine basin (SW France). *Tectonics* 37: 1–20.

Aragüés LMR, Fernández JMG, Fraile DB, de Busto JML, López SG. 1989. Folletto explicativo del mapa geologico de España de Sallent (1/50000). Madrid: Instituto Tecnológico GeoMinero de España.

Barnett-Moore N, Hosseinpour M, Maus S. 2016. Assessing discrepancies between previous plate kinematic models of Mesozoic Iberia and their constraints. *Tectonics* 35: 1843–1862.

Barnolas A, Guérangé B, Chiron JC, Courbouleix S, Autran A, Durand-Delga M, *et al.* 2015. Synthèse géophysique et géologique des Pyrénées 2. AGSO and BRGM.

Bayona G, Cardona A, Jaramillo C, Mora A, Montes C, Caballero V, *et al.* 2013. Onset of fault reactivation in the Eastern Cordillera of Colombia and proximal Llanos Basin; response to Caribbean-South American convergence in early Palaeogene time. *J Geol Soc Lond* 377: 285–314.

Bilotte M. 1984. Les grands foraminifères benthiques du Crétacé supérieur pyrénéen : biostratigraphie. Réflexions sur les corrélations mesogéennes. In: Oertli HJ, ed. Benthos '83: 2nd Int. Symp. On Benthic Foraminifera – Elf Aquitaine, Esso REP and Total CFP, Pau and Bordeaux, pp. 55–60.

Bilotte M. 1985. Le Crétacé supérieur des plates-formes est-pyrenéennes. PhD Thesis. Toulouse (France): Paul Sabatier University.

Bilotte M. 2007. Permanence, au Crétacé supérieur, de la position de la limite plate-forme/bassin dans la zone sous-pyrénéenne orientale (Aude, France) : implications géodynamiques. *Géologie de la France* 1: 33–53.

Biteau J-J, Marrec AL, Vot ML, Masset J-M. 2006. The Aquitaine Basin. *Petrol Geosci* 12: 247–273.

Boix C, Villalonga R, Caus E, Hottinger L. 2009. Late Cretaceous rotaliids (Foraminiferida) from the Western Tethys. *Neues Jahrb Geol P* 253: 197–227.

Boix C, Frijia G, Vicedo V, Bernaus JM, Di Lucia M, Parente M, *et al.* 2011. Larger foraminifera distribution and strontium isotope stratigraphy of the La Cova limestones (Coniacian–Santonian, "Serra del Montsec", Pyrenees, NE Spain). *Cretaceous Res* 32: 806–822.

Bond GC, Kominz MA, Devlin WJ. 1983. Thermal subsidence and eustasy in the Lower Palaeozoic miogeocline of western North America. *Nature* 306: 775–779.

Booler J, Tucker E. 2002. Distribution and geometry of facies and early diagenesis: the key to accommodation space variation and sequence stratigraphy: Upper Cretaceous Congost Carbonate platform, Spanish Pyrenees. *Sediment Geol* 146: 225–247.

Brinkmann RV, Lögters H. 1968. Diapirs in Western Pyrenees and Foreland Spain. *American Association of Petroleum Geologists Memoir* 8: 275–292.

Bronner A, Sauter D, Manatschal G, Péron-Pinvidic G, Munschyn M. 2011. Magmatic breakup as an explanation for magnetic anomalies at magma-poor rifted margins. *Nat Geosci* 4: 549–553.

Burchette TP, Wright VP. 1992. Carbonate ramp depositional systems. *Sediment Geol* 79: 3–57.

Burg J-P, Van Den Driessche J, Brun J-P. 1994. Syn- to post-thickening extension: mode and consequences. *C R Acad Sci II* 319: 1019–1032.

Cámara P, Flinch JF. 2017. The southern Pyrenees: a salt-based fold-and-thrust belt. In: Permo-Triassic Salt Provinces of Europe, North Africa and the Atlantic Margins. Elsevier, pp. 395–415.

Casteras M. 1971. Notice explicative de la carte géologique de Tardets-Sorholus (1/50000). Orléans: Éditions du BRGM.

Casteras M, Villanova M, Godechot Y, Blanc R, Labourguigne J, Deloffre R, *et al.* 1970. Notice explicative de la carte géologique de Lourdes (1/50000). Orléans: Éditions du BRGM.

Catuneanu O, Abreu V, Bhattacharya JP, Blum MD, Dalrymple RW, Eriksson PG, *et al.* 2009. Towards the standardization of sequence stratigraphy. *Earth Sci Rev* 92: 1–33.

Catuneanu O, Galloway WE, Kendall CGSC, Miall AD, Posamentier HW, Strasser A, *et al.* 2011. Sequence stratigraphy: methodology and nomenclature. *Newsl Stratigr* 44: 173–245.

Caus E, Cornella A. 1983. Macroforaminifères du Crétacé supérieur du bassin sud-pyrénéen. *Géologie Méditerranéenne* 10: 137–142.

Caus E, Gómez-Garrido A. 1989. Upper Cretaceous biostratigraphy of the southcentral Pyrenees (Lleida, Spain). *Geodin Acta* 3: 221–228.

Clerc C, Lagabrielle Y, Labaume P, Ringenbach J-C, Vauchez A, Nalpas T, *et al.* 2016. Basement – Cover decoupling and progressive exhumation of metamorphic sediments at hot rifted margin. Insights from the Northeastern Pyrenean analog. *Tectonophysics* 686: 82–97.

Clerc C, Lagabrielle Y, Neumaier M, Reynaud JY, De Saint Blanquat M. 2012. Exhumation of subcontinental mantle rocks: evidence

from ultramafic-bearing clastic deposits nearby the Lherz peridotite body, French Pyrenees. *Bull Soc Géol Fr* 183: 443–459.

Cochelin B, Lemirre B, Denèle Y, de Saint Blanquat M, Lahfid A, Duchêne S. 2017. Structural inheritance in the central pyrenees: the variscan to Alpine tectonometamorphic evolution of the Axial Zone. *J Geol Soc Lond* 175: 336–351.

Curry ME, van der Beek P, Huismans RS, Wolf SG, Muñoz J-A. 2019. Evolving paleotopography and lithospheric flexure of the Pyrenean Orogen from 3D flexural modeling and basin analysis. *Earth Planet Sci Lett* 515: 26–37.

De Grasiansky PC, Dardeau G, Lemoine M, Tricart P. 1989. The inverted margin of the French Alps and foreland basin inversion. In: Cooper MA, Williams GD, eds. Inversion tectonics. Geol Soc Spec Publ 44: 87–104.

Desegaulx P, Brunet M-F. 1990. Tectonic subsidence of the Aquitaine basin since Cretaceous times. *Bull Soc Géol Fr* 2: 295–306.

Dewey JF, Helman ML, Turco E, Hutton DHW, Knott SD. 1989. Kinematics of the western Mediterranean. In: Woward MP, Dietrich D, Park RG, eds. Alpine Tectonics. *Geol Soc Spec Publ* 45: 265–283.

Drzewiecki PA, Simó JA. 1997. Carbonate platform drowning and oceanic anoxic events on a Mid-Cretaceous carbonate platform, south-central Pyrenees, Spain. *J Sediment Res* 67: 698–714.

Drzewiecki PA, Simó JA. 2000. Tectonic, eustatic and environmental controls on mid-Cretaceous carbonate platform deposition, south-central Pyrenees, Spain. *Sedimentology* 47: 471–495.

Drzewiecki PA, Simó JA. 2002. Depositional processes, triggering mechanisms and sediment composition of carbonate gravity flow deposits: examples from the Late Cretaceous of the south-central Pyrenees, Spain. *Sediment Geol* 146: 155–189.

Dubois P, Seguin J-C. 1978. Les flyschs crétacé et éocène de la zone commingeoise et leur environnement. *Bull Soc Géol Fr* 5: 657–671.

Embry A. 2009. Practical sequence stratigraphy. Canadian Society of Petroleum Geologists.

Escalona A, Mann P. 2011. Tectonics, basin subsidence mechanisms, and paleogeography of the Caribbean-South American plate boundary zone. *Mar Petrol Geol* 28: 8–39.

Espurt N, Angrand P, Teixell A, Labaume P, Ford M, de Saint Blanquat M, *et al.* 2019. Crustal-scale balanced cross-section and restorations of the Central Pyrenean belt (Nestes-Cinca transect): highlighting the structural control of Variscan belt and Permian-Mesozoic rift systems on mountain building. *Tectonophysics* 764: 25–45.

Espurt N, Hippolyte J-C., Saillard M, Bellier O. 2012. Geometry and kinematic evolution of a long-living foreland structure inferred from field data and cross section balancing, the Sainte-Victoire System, Provence, France. *Tectonics* 31: TC4021.

Flügel E. 2010. Microfacies of carbonate rocks: analysis, interpretation and implications, 2nd ed. Berlin, New York: Springer-Verlag.

Gaspar-Escribano JM, Van Wees JD, Ter Voorde M, Cloetingh SAPL, Roca E, Cabrera L, *et al.* 2001. Three-dimensional flexural modelling of the Ebro Basin (NE Iberia). *Geophysical J Int* 145: 349–367.

Goldhammer RK. 1997. Compaction and decompaction algorithms for sedimentary carbonates. *J Sediment Res* 67: 26–35.

Gómez-Romeu J, Masini E, Tugend J, Ducoux M, Kusznir N. 2019. Role of rift structural inheritance in orogeny highlighted by the Western Pyrenees case-study. *Tectonophysics* 766: 131–150.

Grool AR, Ford M, Vergés J, Huismans RS, Christophoul F, Dielforder A. 2018. Insights into the crustal-scale dynamics of a doubly Vergent Orogen from a quantitative analysis of its forelands: a case study of the Eastern Pyrenees. *Tectonics* 37: 450–476.

Handy MR, Schmid SM, Bousquet R, Kissling E, Bernoulli D. 2010. Reconciling plate-tectonic reconstructions of Alpine Tethys with the geological-geophysical record of spreading and subduction in the Alps. *Earth Sci Rev* 102: 121–158.

Haq BU. 2014. Cretaceous eustasy revisited. *Glob Planet Change* 113: 44–58.

Haq BU, Hardenbol J, Vail PR. 1987. Chronology of fluctuating sea levels since the Triassic. *Science* 235: 1156–1167.

Hardenbol J, Thierry J, Farley MB, Jacquin T, De Graciansky P-C, Vail PR. 1998. Cretaceous sequence chronostratigraphy – chart 4. In: De Graciansky P-C, Hardenbol J, Jacquin T, Vail PR, eds. Mesozoic and Cenozoic Sequence Stratigraphy of European Basins. *SEPM Special Publication* 60: 3–15.

Hillgärtner H, Strasser A. 2003. Quantification of high-frequency sea-level fluctuations in shallow-water carbonates: an example from the Berriasian-Valanginian (French Jura). *Palaeogeogr Palaeoclimatol Palaeoecol* 200: 43–63.

Hillgärtner H, Dupraz C, Hug W. 2001. Microbially induced cementation of carbonate sands: are micritic meniscus cements good indicators of vadose diagenesis? *Sedimentology* 48: 117–131.

Hottinger L. 1966. Foraminifères rotaliformes et orbitoïdes du Sénonien inférieur pyrénéen. *Eclogae Geol Helv* 59: 277–301.

Hudec MR, Jackson MPA. 2007. Terra infirma: understanding salt tectonics. *Earth Sci Rev* 82: 1–28.

Issautier B, Saspiturry N, Serrano O. 2020. Role of structural inheritance and salt tectonics in the formation of pseudosymmetric continental rifts on the European margin of the hyperextended Mauléon basin (Early Cretaceous Arzacq and Tartas Basins). *Mar Petrol Geol* 118.

Jammes S, Manatschal G, Lavier L, Masini E. 2009. Tectonosedimentary evolution related to extreme crustal thinning ahead of a propagating ocean: example of the western Pyrenees. *Tectonics* 28: 1–24.

Jervey MT. 1988. Quantitative modeling of siliciclastic rock sequences and their seismic expression. *SEPM Spec Publ* 42: 47–69.

Jolivet L, Gorini C, Smit J, Leroy S. 2015. Continental breakup and the dynamics of rifting in back-arc basins: The Gulf of Lion margin. *Tectonics* 34: 662–679.

Jolivet L, Romagny A, Gorini C, Maillard A, Thinon I, Couëffé R, *et al.* 2020. Fast dismantling of a mountain belt by mantle flow: late-orogenic evolution of Pyrenees and Liguro-Provençal rifting. *Tectonophysics* 776: 1–15.

Jourdon A, Le Pourhiet L, Mouthereau F, Masini E. 2019. Role of rift maturity on the architecture and shortening distribution in mountain belts. *Earth Planet Sci Lett* 512: 89–99.

Lacombe O, Angelier J, Laurent P. 1992. Determining paleostress orientations from faults and calcite twins: a case study near the Sainte-Victoire Range (southern France). *Tectonophysics* 201: 141–156.

Lagabrielle Y, Labaume P, de Saint Blanquat M. 2010. Mantle exhumation, crustal denudation, and gravity tectonics during Cretaceous rifting in the Pyrenean realm (SW Europe): insights from the geological setting of the lherzolite bodies. *Tectonics* 29: 1–26.

Lagabrielle Y, Asti R, Duretz T, Clerc C, Fourcade S, Teiwell A, *et al.* 2020. A review of cretaceous smooth-slopes extensional basins along the Iberia-Eurasia plate boundary: how pre-rift salt controls the modes of continental rifting and mantle exhumation. *Earth Sci Rev* 201.

Lasseur E. 2007. La Craie du Bassin de Paris (Cénomanien-Campanien, Crétacé supérieur). Sédimentologie de faciès, stratigraphie séquentielle et géométrie 3D. PhD Thesis. France: Rennes 1 University.

Leleu S. 2005. Les cônes alluviaux Crétacé supérieur/paléocène en Provence : traceurs de l'évolution morpho-tectonique des stades précoces de collision. PhD Thesis. Strasbourg, France: Louis Pasteur University.

Leleu S, Ghienne J-F, Manatschal G. 2009. Alluvial fan development andmorpho-tectonic evolution in response to contractional fault reactivation (Late Cretaceous Palaeocene), Provence, France. *Basin Res* 21: 157–187.

Le Pochat G, Lenguin M, Napias J-C, Thibault C, Roger P, Bois J-P. 1978. Notice explicative de la carte géologique de Saint-Jean-Pied-de-Port (1/50000). Orléans: Éditions du BRGM.

Le Pochat G, Lenguin M, Thibault C. 1976. Notice explicative de la carte géologique de Mauléon-Licharre (1/50000). Orléans: Éditions du BRGM.

López-Mir B, Muñoz JA, García-Senz J. 2014. Restoration of basins driven by extension and salt tectonics: example from the Cotiella Basin in the central Pyrenees. *J Struc Geol* 69: 147–162.

López-Mir B, Muñoz JA, García-Senz J. 2015. Extensional salt tectonics in the partially inverted Cotiella post-rift basin (south-central Pyrenees): structure and evolution. *Int J Earth Sci* 104: 419–434.

Macchiavelli C, Vergés J, Schettino A, Fernàndez M, Turco E, Casciello E, *et al.* 2017. A new Southern North Atlantic Isochron Map: insights Into the Drift of the Iberian Plate Since the Late Cretaceous. *J Geophys Res: Solid Earth* 122: 1–24.

Masini E, Manatschal G, Tugend J, Mohn G, Flament J-M. 2014. The tectono-sedimentary evolution of a hyper-extended rift basin: the example of the Arzacq-Mauléon rift system (Western Pyrenees, SW France). *Int J Earth Sci* 103: 1569–1596.

McKenzie D. 1978. Some remarks on the development of sedimentary basins. *Earth Planet Sci Lett* 40: 25–32.

Merle J-M. 1974. Recherches sur les relations paléogéographiques et structurales entre les massifs basques au sud de Saint-Jean-Pied-de-Port (Pyrénées occidentales). PhD Thesis. France: Toulouse University.

Mey PBW, Nagtegaal PJC, Roberti KJ, Hartevelt JJA. 1968. Lithostratigraphic subdivision of post-hercynian deposits in the southcentral Pyrenees, Spain. *Leidsc Gcologische Mededelingen* 41: 221–228.

Miller KG, Kominz MA, Browning JV, Wright JD, Mountain GS, Katz ME, *et al.* 2005. The Phanerozoic Record of Global Sea-Level Change. *Science* 310: 1293–1298.

Mirouse R. 1962. Recherches géologiques dans la partie occidentale de la Zone primaire axiale des Pyrénées. PhD Thesis. France: Toulouse University, v. 1.

Mouthereau F, Filleaudeau PY, Vacherat A, Pik R, Lacombe O, Fellin MG, *et al.* 2014. Placing limits to shortening evolution in the Pyrenees: Role of margin architecture and implications for the Iberia/Europe convergence. *Tectonics* 33: 2283–2314.

Muñoz JA. 1992. Evolution of a continental collision belt: ECORS-Pyrenees crustal balanced cross-section. In: McClay K, ed. Thrust tectonics. Dordrecht (Netherlands): Springer, pp. 235–246.

Neres M, Front E, Miranda JM, Camps P, Terrinha P, Mirão J. 2012. Reconciling Cretaceous paleomagnetic and marine magnetic data for Iberia: New Iberian paleomagnetic poles. *J Geophys Res Solid Earth* 117: 1–21.

Neres M, Miranda JM, Font E. 2013. Testing Iberian kinematics at Jurassic-Cretaceous times. *Tectonics* 32: 1312–1319.

Ogg JG, Ogg G, Gradstein FM. 2016. A Concise Geologic Time Scale: 2016. Amsterdam: Elsevier.

Olivet J. 1996. La cinématique de la plaque ibérique. *Bull Cent Rech Explor Prod Elf Aquitaine* 20: 131–195.

Papon J-P. 1969. Étude de la zone sud-Pyrénéenne dam le Massif du Turbòn (Prov. de Huesca- Espagne) collision. PhD Thesis. France: Toulouse University.

Philip J, Floquet M, Platel JP, Bergerat F, Sandulescu M, Bara-Boshkin E, *et al.* 2000. Paris: Atlas Peri-Tethys, Palaeogeographical map 14-Late Cenomanian (94.7 to 93.5 Ma). CCGM/CGMW.

Platel J-P. 1987. Le Crétacé supérieur de la plate-forme septentrionale du Bassin d'Aquitain. PhD Thesis. Orléans (France): BRGM.

Platel J-P. 1990. Notice explicative de la feuille de Cazaubon (1/50000). Orléans: Éditions du BRGM.

Plint AG. 2010. Wave- and storm-dominated shoreline and shallow-marine systems. In: James NP, Dalrymple RW, eds. Facies Models 4: GEOtext 6. St. John's, Newfoundland: Geological Association of Canada, pp. 167–199.

Pomar L, Gili E, Obrador A, Ward WC. 2005. Facies architecture and high-resolution sequence stratigraphy of an Upper Cretaceous platform margin succession, southern central Pyrenees, Spain. *Sediment Geol* 175: 339–365.

Poprawski Y, Basile C, Jaillard E, Gaudin M, Lopez M. 2016. Halokinetic sequences in carbonates systems: An example from the Middle Albian Bakio Breccias Formation (Basque Country, Spain). *Sediment Geol* 334: 34–52.

Porthault B. 1974. Le Crétacé supérieur de la « Fosse vocontienne » et des régions limitrophes (France sud-est). PhD Thesis. Lyon, France: Claude Bernard University.

Puigdefàbregas C, Muñoz JA, Vergés J. 1992. Thrusting and foreland basin evolution in the Southern Pyrenees. In: McClay KR, ed. Thrust Tectonics. Dordrecht: Springer, pp. 247–254.

Puigdefàbregas C, Souquet P. 1986. Tecto-sedimentary cycles and depositional sequences of the Mesozoic and Tertiary from the Pyrenees. *Tectonophysics* 129: 173–203.

Razin P. 1989. Évolution tecto-sédimentaire alpine des Pyrénées basques à l'ouest de la transformante de Pamplona (province de Labour). PhD Thesis. France: Bordeaux III University.

Robin C, Guillocheau F, Allemand P, Bourquin S, Dromart G, Gaulier JM, *et al.* 2000. Time and space-scales of the tectonic control on a flexural intracratonic basin: the Paris Basin. *Bull Soc Géol Fr* 171: 181–196.

Rosenbaum G, Lister GS, Duboz C. 2002. Relative motions of Africa, Iberia and Europe during Alpine orogeny. *Tectonophysics* 359: 117–129.

Royden L, Keen CE. 1980. Rifting process and thermal evolution of the continental margin of eastern Canada determined from subsidence curves. *Earth Planet Sci Lett* 51: 343–361.

Sahagian D, Pinous O, Olferiev A, Zakharov V. 1996. Eustatic curve for the Middle Jurassic-Cretaceous based on Russian platform and Siberian stratigraphy: zonal resolution. *AAPG Bull* 80: 1433–58.

Saspiturry N, Razin P, Baudin T, Serrano O, Issautier B, Lasseur E, *et al.* 2019a. Symmetry *vs*. asymmetry of a hyper-thinned rift: example of the Mauléon Basin (Western Pyrenees, France). *Mar Petrol Geol* 104: 86–105.

Saspiturry S, Cochelin B, Razin P, Leleu S, Lemirre B, Bouscary C, *et al.* 2019b. Tectono-sedimentary evolution of a rift system controlled by Permian post-orogenic extension and metamorphic core complex formation (Bidarray Basin and Ursuya dome, Western Pyrenees). *Tectonophysics* 768.

Saspiturry N, Razin P, Allanic C, Issautier B, Baudin T, Lasseur E, *et al.* 2020a. Closure of a hyperextended system in an orogenic lithospheric pop-up, Western Pyrenees: The role of mantle buttressing and rift structural inheritance. *Terra Nova* 00: 1–8.

Saspiturry N, Lahfid A, Baudin T, Guillou-Frottier L, Razin P, Issautier B, *et al.* 2020b. Paleogeothermal Gradients across an Inverted Hyperextended Rift System: Example of the Mauléon Fossil Rift (Western Pyrenees). *Tectonics* 39: 1–36.

Saspiturry N, Issautier B, Razin P, Baudin T, Asti R, Lagabrielle Y, *et al.* 2021, Review of Iberia-Eurasia plate-boundary basins: role of sedimentary burial on depth-dependent continental crust ductile thinning during rifting and continental breakup. *Bassin Res* 33: 1626–1661.

Saura E, Oró i Ardèvol L, Teixell A, Vergès J. 2016. Rising and falling diapirs, shifting depocenters, and flap overturning in the Cretaceous Sopeira and Sant Gervàs subbasins (Ribagorça Basin, southern Pyrenees). *Tectonics* 35: 638–662.

Schlager W. 1993. Accommodation and supply − a dual control on stratigraphic sequences. *Sediment Geol* 86: 111–136.

Schlager W. 2004. Fractal nature of stratigraphic sequences. *Geology* 32: 185–188.

Schlager W. 2005. Carbonate Sedimentology and Sequence Stratigraphy. In: SEPM Concepts in Sedimentology and Paleontology.

Serrano O. 2001. Le Crétacé supérieur-Paléogène du basin compressif nord-pyrénéen (Bassin de l'Adour) : sédimentologie, stratigraphie, géodynamique. PhD Thesis. France: Rennes I University.

Sibuet JC, Srivastava SP, Spakman W. 2004. Pyrenean orogeny and plate kinematics. *J Geophys Res Solid Earth* 109: 1–18.

Simó JA. 1986. Carbonate platform depositional sequences, Upper Cretaceous, south-central Pyrenees (Spain). *Tectonophysics* 129: 205–231.

Simó JA. 1993. Cretaceous carbonate platforms and stratigraphic sequences, south-central Pyrenees, Spain. In: Simó JA, Scott RW, Masse J-P, eds. Cretaceous Carbonate Platforms. *American Association of Petroleum Geologists, Memoir* 56: 325–342.

Sinclair HD, Naylor M. 2012. Foreland Basin Subsidence Driven by Topographic Growth versus Plate Subduction. *Geol Soc Am Bull* 124: 368–79.

Skelton PW, Gili E, Vincens E, Obrador A, López YG. 2003. Revised lithostratigraphy of the Upper Cretaceous (Santonian) carbonate platform succession on the northern flank of Sant Corneli, southern Central Pyrenees. *J Iber Geol* 29: 73–87.

Souquet P. 1967. Le Crétacé supérieur sud-pyrénéen en Catalogne, Aragon et Navarre. Thèse d'état. France: Toulouse Science Faculty.

Souquet P, Peybernès B, Bilotte M, Debroas E-J. 1977. La chaîne alpine des Pyrénées. *Géologie Alpine* 53: 193–216.

Srivastava S, Sibuet J-C., Cande S, Roest W, Reid ID. 2000. Magnetic evidence for slow seafloor spreading during the formation of the Newfoundland and Iberian margins. *Earth Planet Sci Lett* 182: 61–76.

Steckler MS, Watts AB. 1978. Subsidence of the Atlantic-type continental margin off New-York. *Earth Planet Sci Lett* 41: 1–13.

Teixell A. 1996. The Ansó transect of the southern Pyrenees: basement and cover thrust geometries. *J Geol Soc Lond* 153: 301–310.

Teixell A, Garcia-Sansegundo J, Zamorano M, Caus E, Robador A, Remacha E, *et al.* 1994. Folletto explicativo del mapa geologico de España de Ansó (1/50000). Madrid: Instituto Tecnológico Geo-Minero de España.

Teixell A, Labaume P, Ayarza P, Espurt N, de Saint Blanquat M, Lagabrielle Y. 2018. Crustal structure and evolution of the Pyrenean-Cantabrian belt: A review and new interpretations from recent concepts and data. *Tectonophysics* 724–725: 146–170.

Teixell A, Labaume P, Lagabrielle Y. 2016. The crustal evolution of the west-central Pyrenees revisited: Inferences from a new kinematic scenario. *C R Geosci* 348: 257–267.

Tempier C, Durand JP. 1981. Importance de l'épisode tectonique d'âge Crétacé supérieur dans la structure du versant méridional de la montagne Sainte-Victoire (Proverice). *C R Acad Sci Paris* 293: 629–632.

Ternet Y. 1965. Étude du synclinal complexe des Eaux-Chaudes (Basses Pyrénées). PhD Thesis. France: Toulouse University.

Ternet Y, Majesté-Menjoulas C, Canerot J, Baudin T, Cocherie A, Guerrot C, *et al.* 2004. Notice explicative de la carte géologique de Laruns-Somport (1/50000). Orléans: Éditions du BRGM.

Ternois S, Odlum M, Ford M, Pik R, Stockli D, Tibari B, *et al.* 2019. Thermochronological Evidence of Early Orogenesis, Eastern Pyrenees, France. *Tectonics* 38: 1308–1336.

Tugend J, Manatschal G, Kusznir NJ, Masini E. 2014. Characterizing and identifying structural domains at rifted continental margins: application to the Bay of Biscay margins and its Western Pyrenean fossil remnants. *Geol Soc Spec Publ* 413: 171–203.

Tugend J, Manatschal G, Kusznir NJ. 2015. Spatial and temporal evolution of hyperextended rift systems: Implication for the nature, kinematics, and timing of the Iberian-European plate boundary. *Geology* 43: 15–18.

Vacherat A, Mouthereau F, Pik R, Huygues D, Paquette J-L, Christophoul F, *et al.* 2017. Rift-to-collision sediment routing in the Pyrenees: a synthesis from sedimentological, geochronological and kinematic constraints. *Earth Sci Rev* 172 43–74.

Vergés J. 1993. Estudi geològic del vessant Sud del Pirineu Oriental i Central: Evolució en 3D. PhD Thesis. Spain: Universitat de Barcelona.

Vergés J, Marzo M, Santaeulària T, Serra-Kiel J, Burbank DW, Muñoz JA, *et al.* 1998. Quantified vertical motions and tectonic evolution of the SE Pyrenean foreland basin. *London Geological Society Special Publications* 134: 107–134.

Vergés J, Millán H, Roca E, Muñoz JA, Marzo M, Cirés J, *et al.* 1995. Eastern Pyrenees and related foreland basins: pre-, syn and post-collisional crustal-scale cross-sections. *Mar Petrol Geol* 12: 903–915.

Vergés J, Mufloz JA, Martfnez A. 1992. South Pyrenean fold-and-thrust belt: role of foreland evaporitic levels in thrust geometry. In: McClay KR, ed. Thrust Tectonics. London: Chapman & Hall, pp. 255–264.

Vincens E, López G, Obrador A. 1998. Facies succession, biostratigraphy and rudist faunas of Coniacian to Santonian platform deposits in the Sant Corneli anticline (southern central Pyrenees). *Geobios* 22: 403–427.

Vissers R, Meijer PT. 2012. Mesozoic rotation of Iberia: Subduction in the Pyrenees? *Earth Sci Rev* 110: 93–110.

Xie X, Heller PL. 2009. Plate tectonics and basin subsidence history. *Geol Soc Am Bull* 121: 55–64.

Cite this article as: Andrieu S, Saspiturry N, Lartigau M, Issautier B, Angrand P, Lasseur E. 2021. Large-scale vertical movements in Cenomanian to Santonian carbonate platform in Iberia: indicators of a Coniacian pre-orogenic compressive stress, *BSGF - Earth Sciences Bulletin* 192: 19.